Freie Universität Berlin

Summerschool 2017

Modeling of Mass and Energy Transport in Porous Media

Physical Basics

In memoriam *Ulf Bayer*

F. Magri

Introductory remarks

Newton's physics or classical mechanics is based on balance equations or conservation laws, like the preservation of mass, energy, and momentum etc. Also the quantities involved in the theory had in parts already studied by Galilei, Kepler, Descartes, and Huygens, it was on Newton (1687) to define the proper relations and to built a first unique system. The only exception was the conservation of energy, a law which was only recognized since the middle of the 19th century by Mayer, Joule and independently by Helmholtz. The strange point is that the conservation of energy was experimentally first proved in the early 20th century, at a time when the Newtonian physics was already overcome by relativity theory.

In order to integrate previous observations in a concise theory, Newton also developed one form of differential calculus calling the new method the fluxeon theory, obviously motivated by physics in terms of flows (fluxes). At the same time Leibnitz invented his more formal way for defining differentials and the differential calculus, a parallel development which caused a dispute about the ownership between the two opponents for all their lifetime. However, despite their dispute, a new powerful tool had developed, which can be elucidated by the concept of the

Black Box Analogy
Consider you get some electrical devise with two pairs of terminals, one marked input and the other one output. And, you are not able to open the devise; otherwise it would be disturbed (not unreasonable if you consider a computer chip). What you can do is to connect a defined source at the input and to observe the output, let say by an oscilloscope which displays the output current as a function of time. Then by knowing the rules of electricity you may try to find a circuit which is equivalent to the content of the devise. By example, assuming the content consists of a coil of induction and a resistance as shown,

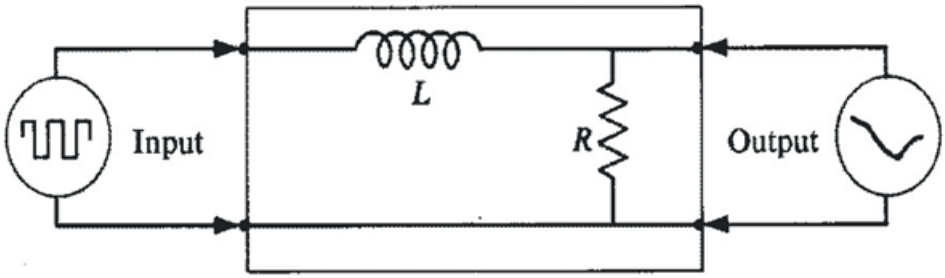

Then the current I satisfies the differential equation

$$L\frac{di}{dt} + Ri = e(t),$$

e(t) is the input voltage. By solving the equation formally you can test whether your hypotheses about the content is verified by some combination of L and R values, otherwise you may try another configuration unless you derived a model about the unknown processes within the box.

During the 18th century a branch of physics developed which did not focus mainly at finite objects considered in addition continua (e.g. Euler). However, essential results concerning the integration of observations and theory where only achieved during the 19th century, e. g. the concept of the stress tensor was developed by Cauchy also he still tried to unify it with popular concepts of particle interaction, Navier and Stokes developed the theory of viscous flow which in principle solved basic problems of the insufficient Euler equations but even

today provide serious problems concerning their solutions, or Kirchhoff formulated the precise theory of bending a beam for which before twice an award was proposed by the French National Academy of Sciences. In other areas a closed theory, or even the basic experiment, was only established during the early 20th century.

When Newton and Leibnitz invented the differential calculus, they found a strong opposition in the church because some infinitely small simply could not exist. This problem was still not really overcome in the 19th century and sometimes it is still showing up today, not at least in connection with porous media. As mentioned, Navier tried to relate his flow equations to the interaction of particles and failed. Similar, until today, attempts are undertaken to derive flow in porous media from first principles at the microscopic level with more or less success. Obviously a porous medium consists of solids and pores as illustrated in the sketch and the flow is naturally restricted to the pores.

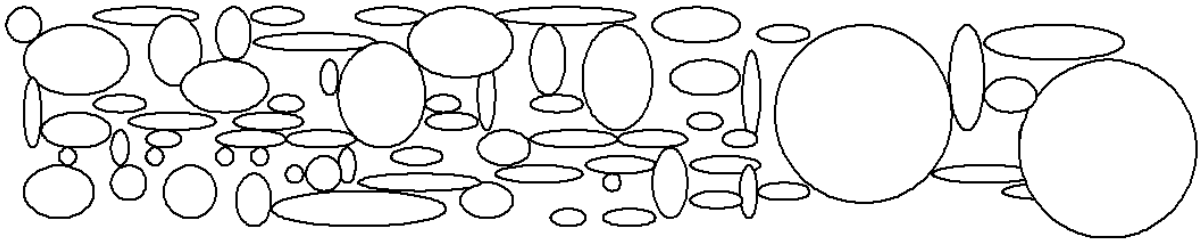

In this case differentiability obviously seems to be violated in terms of what one has learned in terms of differentiable functions which now should be applied to two or even three dimensions. However, as will turn out below that's not really a problem if we consider a so called

Characteristic Volume

Consider we take randomly very small probes like 1 mm^2 from the idealized porous medium sketch above, we will find basically two separated samples, one just consisting of rock and the other one representing just fluid within the pore, between these extremes we will find very few samples consisting partly of rock and partly of fluid. Now, by increasing the sampling area or volume continuously we will find less and less samples which contain only one of the extremes and increasingly more containing a certain fraction of both states. While increasing the size of the sample volume, the variance of the resulting probability distribution will decrease and approach a rather sharp peak. Whenever the sample size has grown to a volume for which the variance approaches zero, we can talk about the characteristic volume because the parameter under consideration can be precisely predicted from a single sample.

This at least theoretical approach is illustrated in the figure below, where the average conductivity for an artificial material produced in the computer has been calculated. The material is composed of the two extreme states totally conductive (1) and totally isolating (0) and the measured variability of observed conductivities is plotted against the characteristic volume measured in pixels.

Artificial sedimentological patterns

fraction of material 2 (red): 0.40

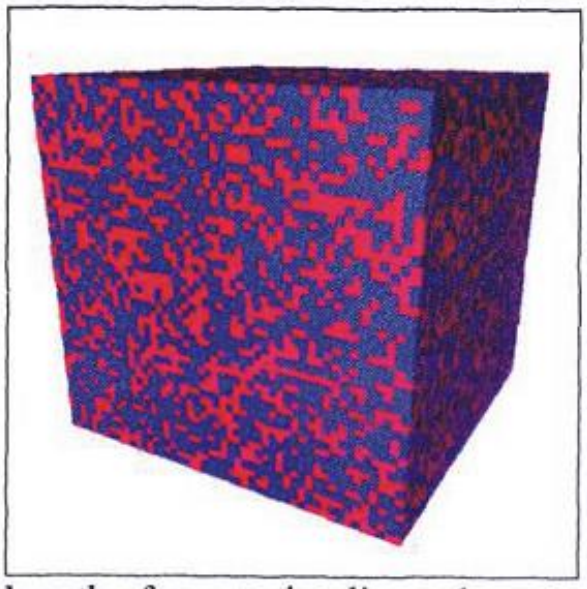

length of generating line = 1

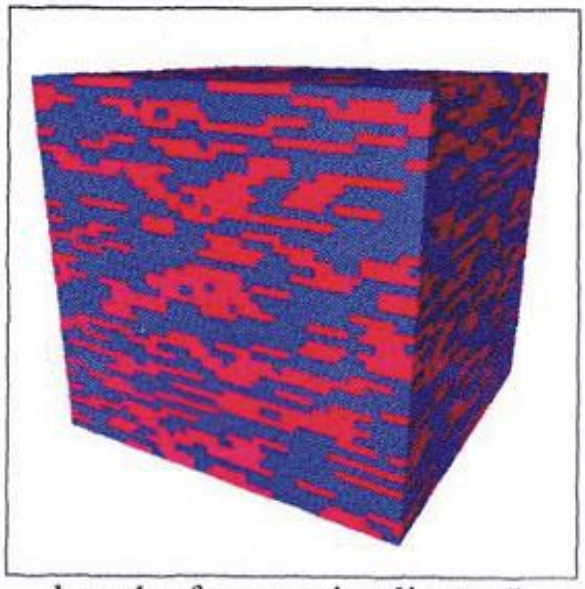

length of generating line = 5

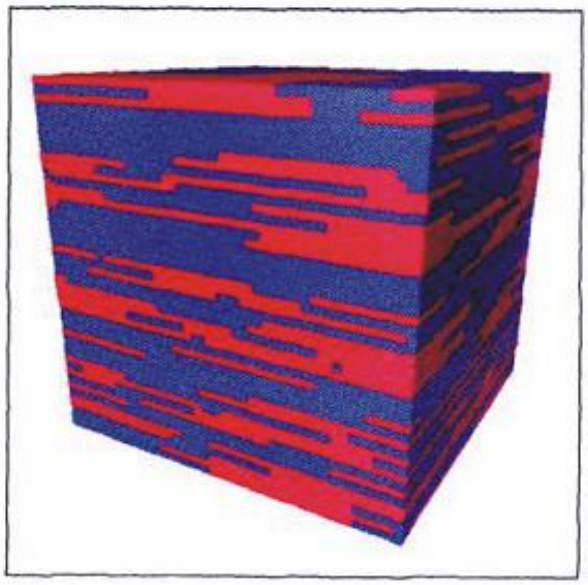

length of generating line = 10

length of generating line = 50

Varianz of calculated conductivity

related to bitmap size

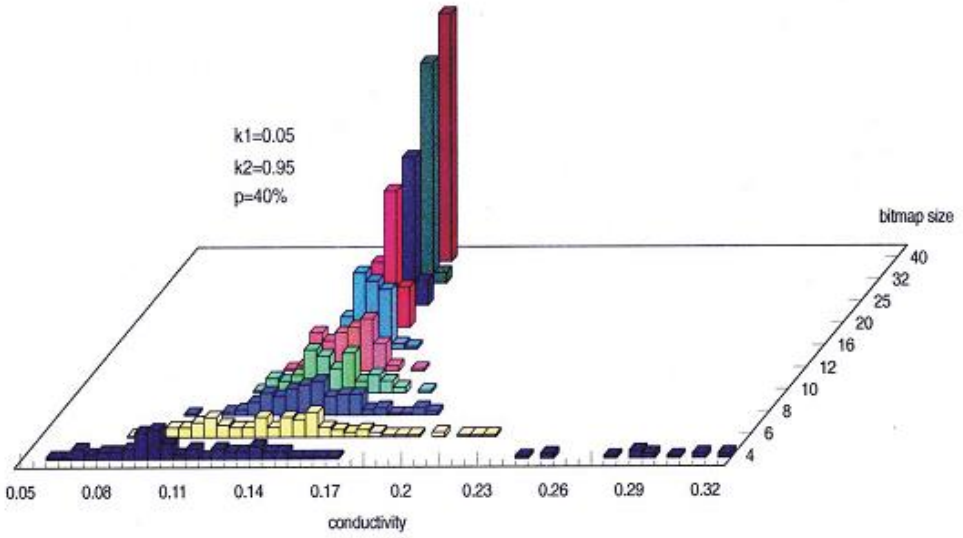

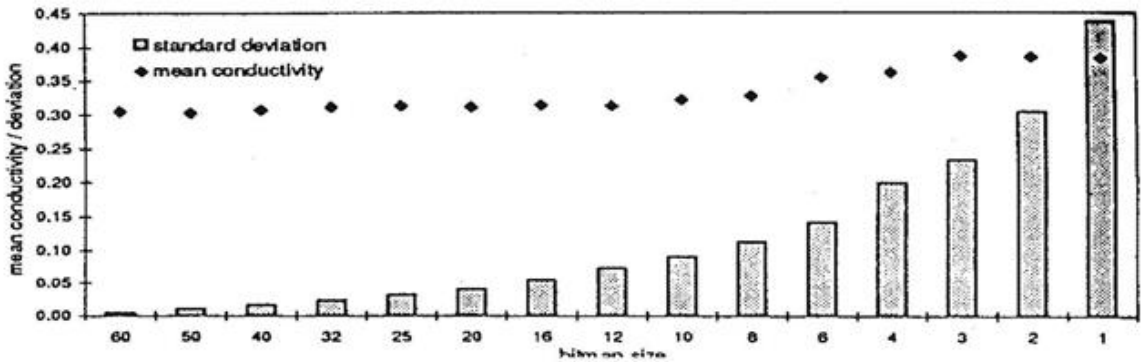

Chapter 2: Mass and Energy Balance, Basics

In textbooks on porous flow you may find either just the governing differential equations or some difference scheme is derived from a simple rectangular area. In a physical sense any geometrical restriction to a control volume is not acceptable because otherwise you could not be sure that your result, in our case partial differential equations, is of general nature. Nevertheless, we start with some simple geometrical objects to clarify basics before entering into a more general description.

Let's consider a simple parallel flux field (vector field) within the area G which may represent some mass or energy transport or even some force as illustrated in the following sketch.

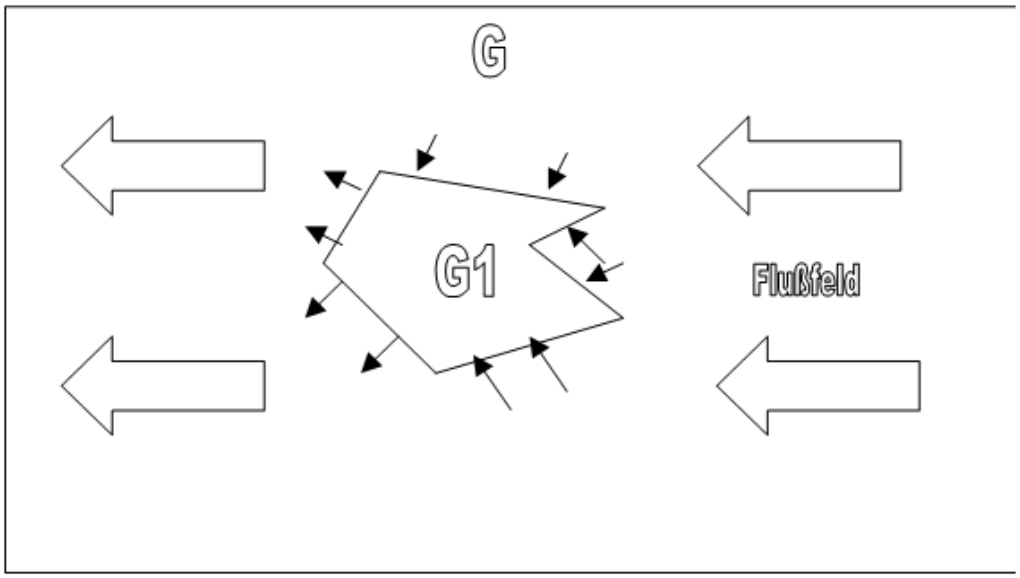

From G we cut a sub area G1 bounded by an arbitrarily closed polygon. The simple question to be solved then is whether the inflow is balanced with the outflow or, perhaps, does something happen inside. In order to calculate the amount entering or leaving we have to consider every surface element and to divide the flux vector into a component perpendicular to the surface, the amount entering, and a second one parallel to the surface element, indicating the amount bypassing. Because we will similar considerations later on, lets do that as an

Exercise
Given a flux vector, this is approaching an oblique oriented surface element (line) of your choice. Separate it graphically into the flux components parallel and oblique to the surface:

The graphic procedure, however, is not really satisfying. In order to derive a computational scheme one defines the normal vector to the surface element. There are three rules or simply definitions necessary in order to avoid confusion:

The normal vector of a surface element for a closed area satisfies the conditions

1) *The normal is perpendicular to the surface.*
2) *The normal vector points to the outside of the closed are.*
3) *The closed area is always surrounded anticlockwise.*

Given the normal vector, the fluxes entering into the area are simply calculated by
$\vec{v}_{in} = -\vec{n}\vec{v}$.
In order to understand the negative sign we consider the rather simple configuration where at the left all fluxes (black) are directed outside while at the right they are all directed inward.

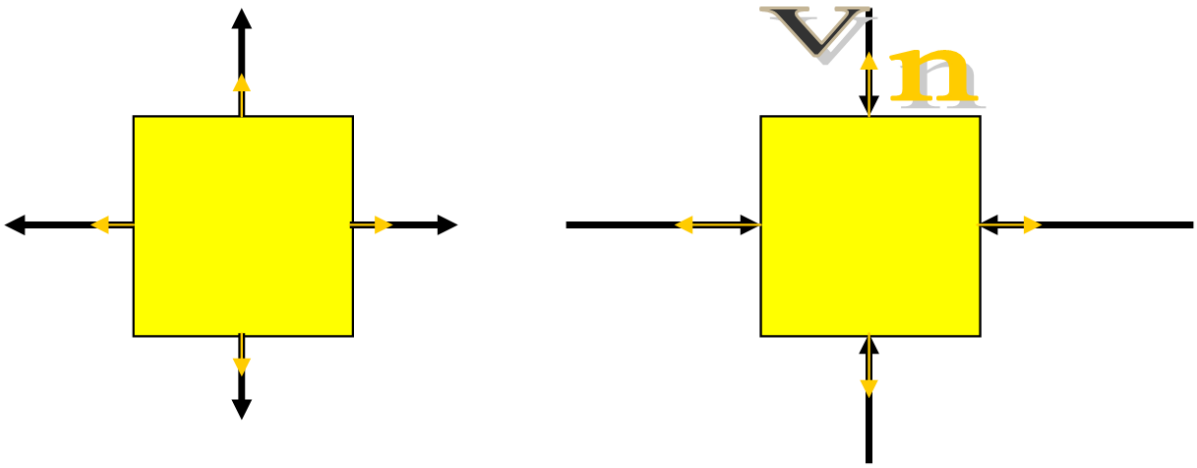

In this special case and in the two-dimensional projection, the normal vectors of the surface are given by (consider the anticlockwise rule)

$\vec{n}_i = (1,0),(0,1),(0,-1),(-1,0)$.
The fluxes for the left case are
$\vec{v}_i = (a,0),(0,a),(0,-a),(-a,0)$
Taking the sum over the scalar products $\vec{v}_i\vec{n}_i$ over the surface areas (which are L_i , L=the length of the bounding area element) we get the total flux

$$\sum \vec{v}_i\vec{n}_i L_i = 4\vec{v}\vec{n}L,$$

although all fluxes are leaving the area under consideration. So if we take the view from inside the control area the change within the area is correctly described by

$$\text{change} = -\sum \vec{v}_i\vec{n}_i L_i$$

or in terms of a continuous differentiable surface we get the surface integral
$\text{change} = -\oiint_S \vec{v}\vec{n}ds$.

NOTE: The change observed within the area under consideration obviously is a scalar value while the input to our 'black box' is a vector field!

Exercise
Show that the results are the same for the case of fluxes entering the area, as illustrated by the right cube in the sketch.

Fluxes derived from a potential

In many cases the fluxes are derived from a scalar field which frequently satisfies the conditions of a potential field $\Omega(x, y, z)$. The gradient of such a scalar field generates a vector field or more precisely the gradient field

$$\vec{j} = grad\Omega$$

or in Cartesian coordinates

$$\vec{j} = \nabla\Omega$$

In this case $\vec{j}$ measures the slope of the scalar field and has a positive value if the height of the surface increases in the neighborhood of the point under consideration. ´The sketch below illustrates two special cases with regard to local coordinates: At the left the point under consideration sitting on a ridge and at the right at the bottom of a valley.

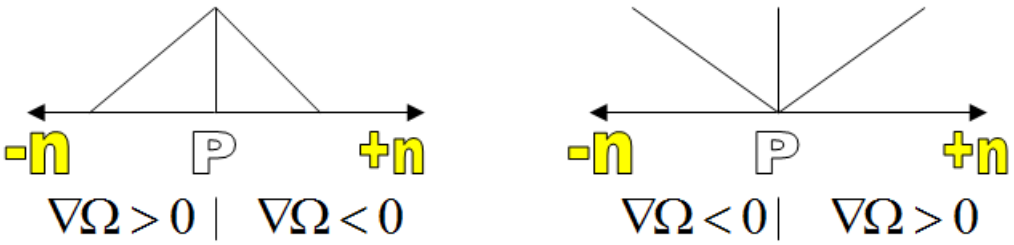

The sign of $\nabla\Omega$ is hill upward positive while the transport always should be hill downward in order to satisfy the minimum principle of energy. The fluxes, therefore, are opposite to the gradient of the scalar function

$$\vec{v} = -grad\Omega$$

or

$$\vec{v} = -\nabla\Omega,$$

and the Balance equations become

$$\text{change} = -\sum -grad(\Omega_i)\vec{n}_i L_i \;=\; \sum grad(\Omega_i)\vec{n}_i L_i$$

or

$$\text{change} = -\oiint_S -grad(\Omega)\vec{n}ds \;=\; \oiint_S grad(\Omega)\vec{n}ds\,.$$

Summary
If we consider an arbitrary bounded area within a flux field, the changes within this are or the difference between in and outgoing fluxes is given by

$$\nabla\vec{v} = \vec{v}_{out} - \vec{v}_{in} \;= -\oiint_S \vec{v}\vec{n}ds \;=\; \oiint_S grad(\Omega)\vec{n}ds\,.$$

Now, the balance equation derived depends on the size or volume of our control volume V. In order to make it comparable to other materials, by example, we have to normalize it

$$(\nabla\vec{v}/V = (j_{out} - j_{in})/V .$$

$\nabla\vec{v}$ defines what happens within the area under consideration:

$\nabla\vec{v} > 0$	something is produced:	source
$\nabla\vec{v} = 0$	nothing happens:	flow equilibrium
$\nabla\vec{v} < 0$	something is consumed:	sink.

The Divergence Theorem

We already considered the need of normalizing our control volume. In a more mathematical sense we may also consider a small volume V surrounding a point M. Then by reducing the volume we will arrive finally at the value of change taking place at the point itself, leading to the divergence at that point

$$div(\vec{v}) = \lim_{V \to M} \frac{\oiint \vec{v} ds}{V} .$$

We will see later, that this limit is not necessary to derive the appropriate differential equations otherwise we would restrict ourselves to homogeneous media not in agreement with porous media. Nevertheless, the following exercise is useful:

Exercise

Show in the one-dimensional case that $div(\Omega) = \frac{v_{out} - v_{in}}{\Delta l} = \frac{d^2\Omega}{dx^2}$ *and for a rectangular cube that* $div\Omega = \nabla^2\Omega$*, even in three dimensions.*

The Gauss or Gauss-Ostrogradadski Formula

Without prove we give the following important relation known as Gauss formula:

$$\iiint_V \nabla\vec{v} dV = \oiint_S \vec{v}\vec{n} ds$$

where $\vec{v}$ indicates the vector field of fluxes and $\vec{n}$ the normal vector of the surface, the scalar product $\vec{v}\vec{n}$ is the projection of $\vec{v}$ onto $\vec{n}$.

Here a surface integral within a vector field is related to a volume integral and vice versa. This will be used in deriving the governing partial differential equations and it provides the base for Greens formulae which play an essential role in the FE-method.

Gauss Theorem and Green's Formulae

Let G be an area bounded by piecewise smooth surface elements, then we find

a) Given the continuous vector field v=(U(x,y,z), V(x,y,z), W(x,y,z)) within G, then we have by the Gauss' theorem

$$\iiint_G \nabla v \, dg = \oiint_S v * n \, ds \, .$$

b) Now let's write $U = \Psi F, \quad V = \Psi G, \quad W = \Psi H$ *or* $u = \Psi v$,
where Ψ, F, G, H are functions of (x,y,z), then

$$\iiint_G v \nabla \Psi dg = -\iiint_G \psi \nabla v dg + \oiint_S \psi (v * n) ds$$

c) Another special case is derived if the vector v(F,G,H) is the gradient of a scalar field (e.g. temperature, pressure, concentration), $v = \nabla \Phi$:

$$\iiint_G \Psi \nabla^2 \Phi dg = -\iiint_G (\nabla \Psi) * (\nabla \Phi) dg + \oiint_S \Psi (\nabla \Phi) * n \, ds$$

and in case of $\Psi = c = const.$:

$$\iiint_G \nabla^2 \Phi dg = \oiint_S (\nabla \Phi) * n \, ds \, .$$

These equations play a significant role in deriving FE and FV methods from partial differential equations.

Mass and Energy Balance continued

During the previous discussion we have seen that the surface integral within a flux field $\vec{v}$, taken over a specific control volume provides a scalar value. Considering that this value results from a not necessarily continues scalar field u within the control volume we can consider its temporary change which at any instance has to be equal to the difference between the in- and outflow:

$$\frac{d}{dt}\iiint_V u dV = -\oiint_S \vec{v}\vec{n} ds$$

Provided the control Volume(s) under consideration does not change we can write

$$\iiint_V \frac{\partial u}{\partial t} dV = -\oiint_S \vec{v}\vec{n} ds$$

and by use of the Gauss Theorem the right hand side can be rewritten as

$$\iiint_V (\frac{\partial u}{\partial t} + div(\vec{v}))dV = 0 ,$$

or

$$\iiint_V (\frac{\partial u}{\partial t} + div(\vec{v}))dV = 0$$

in case there is no gain or loss within the control volume. Otherwise we have some production or destruction Q which has to be measured as [value/time unit] and we have to consider

$$\iiint_V \frac{\partial u}{\partial t} dV + \iiint_V \pm Q dV = -\iiint_V div(\vec{v}) dV$$

with Q positive in the case of production and negative in case of destruction. Summarizing this case we get

$$\iiint_V (\frac{\partial u}{\partial t} + div(\vec{v}) \pm Q)dV = 0$$

KEY QUESTION
Under which conditions will the equality in the equations

$$\iiint_V \left(\frac{\partial u}{\partial t} + div(\vec{v})\right) dV = 0$$

and

$$\iiint_V \left(\frac{\partial u}{\partial t} + div(\vec{v}) \pm Q\right) dV = 0$$

hold, independent of the size of the control volume?
Please state:

Note: You should end up with a differential equation without using the divergence theorem or any consideration of a limit as V->0.

Remark 1
The assumption that the control volume does not change is a first order approximation for sedimentary sequences. During continuous sedimentation the overload increases and the sediments will compact just due to mechanical forces, or equivocally, the volume will decrease during time. In addition, chemico-physica processes like pressure solution and redistribution may occur which complicate the stress dependent processes in addition. To consider this aspect is beyond the present scope.

Remark 2
The equation

$$\iiint_V \left(\frac{\partial u}{\partial t} \pm Q\right) dV = -\oiint_S \vec{v}\vec{n} ds$$

where Q may be zero, provides a weak formulation of the problem to solve transport processes. For that purpose subdivide the area under consideration into aerial subsets, by example triangles as illustrated in the sketch

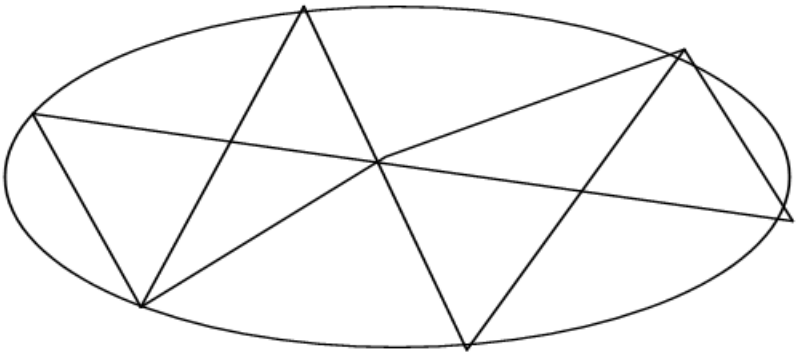

Then we can evaluate the volume integral e. g. by using the Gauss theorem and we can formally evaluate the fluxes through the bounding lines or surfaces. An interesting aspect is that, by considering the anti clockwise rule for the surface integral all internal boundaries vanish. This is equivalent to the statement that the flow leaving one internal volume element along boundary i has to be equal to the flux entering the neighboring element along the same boundary. Or in other words, the mechanism ensures the conservation of the property u within the area under consideration as long as nothing is lost during the outer boundary indicated as an ellipse in the sketch. The equation of course does not include a rule how to calculate the flux at the boundaries between elements or the scalar u within the elements. This final problem is the topic of numerical mathematics and is differently done by example in Finite Differences (FD), Finite Volumes (FV) or Finite Elements (FE).

The equation

$$\iiint_V \left(\frac{\partial u}{\partial t} + div(\vec{v}) \pm Q\right) dV = 0$$

is certainly satisfied if

$$\frac{\partial u}{\partial t} + div(\vec{v}) \pm Q = 0 \quad \text{or} \quad u_t + \nabla\vec{v} \pm Q = 0$$

holds for every point within the area under consideration. Consider the case of a porous medium and $\vec{v}$ the pore water flux. Certainly, within the solids nothing is flowing and all parts of the differential equation have to evaluate to zero. Within the pores flow occurs satisfying the differential equation.

If $\vec{v}$ is derived from a scalar field or potential Ω, i. e. $\vec{v} = -grad\Omega$ the equations become

$$\frac{\partial u}{\partial t} - div(grad\Omega) \pm Q = 0 \quad \text{or} \quad u_t - \nabla^2\Omega \pm Q = 0$$

In case there is no temporal change or production within our 'black box', the equation reduces to the Laplace equation

$$\nabla^2\Omega = 0$$

which played an essential role before digital computers had become available. First, some fundamental solutions are known for the Laplace equation basic solutions are known, especially in two dimensions, and from these solutions for more complex areas can be derived by conformal maps.

The differential equations derived, obviously cannot be solved because we lack a relation between u and $\vec{v}$. We will return to this problem below. However, not even the Laplace equation can be solved unless we define an area with closed boundaries and additional conditions along the boundary. There are two basic and one derived boundary conditions:

- ***1st kind or DIRICHLET's condition: Find a harmonic solution for the interior of the considered area so that the solution*** $\Omega(x, y, z)$ ***satisfies given values of*** $\Omega = f(s)$ ***along the boundary.***
- ***2nd kind or NEUMANN's condition: Find a harmonic solution for the interior of the considered area so that the solution*** $\Omega(x, y, z)$ ***satisfies given values of the normal derivative*** $\frac{\partial\Omega}{\partial n} = f(s)$ ***along the boundary.***
- ***3rd kind or mixed condition: Find a solution for the interior of the considered area so that the solution*** $\Omega(x, y, z)$ ***satisfies the equation*** $\alpha\Omega + \beta\frac{\partial\Omega}{\partial n} = f(s)$, ***and*** $(\alpha, \beta = const, \alpha^2 + \beta^2 \neq 0)$ ***along the boundary.***

In case of the time dependent equation, we obviously need additionally an initial condition within the area under consideration, i.e. the state from which the process starts. Observe that this state has not to satisfy the differential equation and that the solution for very long time will be determined by the boundary conditions.

Exercises

1) *Find (qualitatively) the solution for the 1-D problem* $\frac{\partial u}{\partial x} = 0$ *with u=a at x=0 and u=b at x=1.*
2) *What would be the solution over a square with values of u given at the four corner points?*
3) *How can the boundary condition* $\frac{\partial u}{\partial n} = 0$ *be interpreted (2 possibilities).*
4) *Consider a well located within a homogeneous aquifer with free surface. The well has diameter* ***r*** *and you are pumping continuously* ***Q*** *[m^3] water. The free water surface within the well than will have dropped to height* ***H***. *Through the surface area of the well water will flow* ***v*** *[m/s]which is proportional to the slope of the free water surface or* $v = K\frac{\partial y}{\partial x}$, *with y the height of the free water surface. At the boundary of the well the water level in the aquifer will be equal to the free water level within the well. Derive the differential equation, the required boundary conditions and the solution. Sketch the solution.*

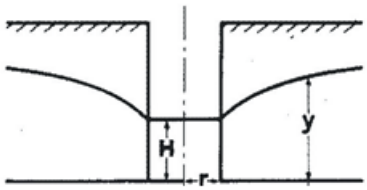

Notation of Differentials

Let U be a scalar function U(x,y,z), then

$\nabla U = gradU = (\frac{\partial U}{\partial x}, \frac{\partial U}{\partial y}, \frac{\partial U}{\partial z}) = (U_x, U_y, U_z)$ generates a vector.

∇ : *NablaOperator*
grad: the gradient, in euclidean space equivalent to ∇.

The *Nabla* operator is used like a vector, i.e. the rules of vector algebra apply:

$$\nabla^2 = \nabla * \nabla = \frac{\partial^2}{\partial x^2} + \frac{\partial^2}{\partial y^2} + \frac{\partial^2}{\partial z^2} = \Delta$$

or, if the operator is applied twice, a scalar field results. Alternatively the Divergence *div* or the Δ : *LaplaceOperator*. are used

$$\nabla^2 U = \frac{\partial^2 U}{\partial x^2} + \frac{\partial^2 U}{\partial y^2} + \frac{\partial^2 U}{\partial z^2} = \Delta U = div(gradU) = U_{xx} + U_{yy} + U_{zz}$$

Chapter 3: Fluxes and Special Partial Differential Equations

The divergence or Gauss theorem provides us with an abstract relationship between a state and a flux, however, not with an equation which could be solved unless we find a functional relationship between the two properties. Concerning the fluxes, these relationships are based on experience (experiments) which are performed on a representative volume. By example, consider a coarse grained rock like granite and its heat conduction. If you perform your experiment at a very small volume you may measure just from a feldspar or a quartz grain, only if your volume is 'representative' you will get the average value for the rock rather than a single type of mineral. There have been and there are many attempts to solve the so called up scaling problem that means to derive large scale properties from rather small scale or even microscopic ones. Although this attempt in is fascinating in itself, mostly it is not very practical and well designed experiments are more successful. First attempts in this direction have been made in 50^{th} of the 19^{th} century in terms of the theory of irreversible thermodynamic processes. However, the closure with classical thermodynamics was never fully established. Here we will consider only rather simple examples with the fluxes derived from a scalar field or potential, sufficient for the problems considered here.

Fick's 1st law is describing the redistribution of a soluble chemical species within a fluid in the sense of the continuums theory. The flux is

$\vec{j}_c = -D\nabla C$,

C is the concentration of the substance and D is the Diffusion coefficient. Obviously C is a scalar property while D may be a tensor if the medium is anisotropic. In this case we can derive an explanation from classical thermodynamics, especially the Brownian motion; however, one cannot explain an initial disturbance within the frame of the classical theory. The flux then is related to the temporal change observed by

$$\frac{\partial \phi C}{\partial t} = \nabla(D\nabla C)$$

or if we have to consider chemical reactions between the solid and fluid indicated by Q

$$\frac{\partial \phi C}{\partial t} \pm Q = \nabla(D\nabla C);$$

φC is the volume of fluid within the porous medium. In addition, consider the previous arguments.

Exercise
***C** can be, dependent on the purpose be defined in different units, e.g. **Vol%** (e.g. spirits), **g/l or kg/m^3** , oralternatively **mol/l**. Dependent on the definition the dimension of the diffusion coefficient **D** will be modified. The rule, however, is that the dimension at the left side has to be identical with the dimension of the right side of the equation, a statement which always has to be true. Derive the dimension of **D** for the different measurements mentioned.*

Based on the previous equation one can elucidate how fluxes derived from a potential are related to random processes which may occur on the microscopic level and how they even may affect numerical solutions.

Consider we have two areas with different diffusion coefficients $D_1 < D_2$ and we add some concentrated solute (say as Dirac delta function) right at the boundary, then by our flow law the material will move faster into area (2) than area (1). The spreading process of the particles can be described by a simple Markov process; however, we have to consider that the distance any particle will move per time unit (speed) depends on the area where it is moving. The

distance in D_1 will be proportional to D_1 / D_2 if we select the distance of grid points as 1 within D_2. Thus, the problem to solve the spreading process into areas of different permeabilities by a random model is simply solved by transforming the distance between discrete grid points to which particles may jump within one time unit, with the distances being proportional to the ratio of the diffusion coefficients.

Alternatively we may derive a finite difference scheme for solving the stationary equation $\nabla(D\nabla C) = 0$, which we can write as

$$\{\frac{D_2(C_2 - C_1)}{\Delta x} - \frac{D_1(C_1 - C_0)}{\Delta x}\}/(\Delta x) = 0$$

or by changing the distance between grid points by the transformation $\Delta x_2 = \Delta x / D_2; \Delta x_1 = \Delta x / D_1$ we get

$$\{\frac{(C_2 - C_1)}{\Delta x_2} - \frac{(C_1 - C_0)}{\Delta x_1}\}/(\frac{\Delta x_2 + \Delta x_1}{2}) = 0.$$

In the first case the equation looks symmetrical and one may conclude that the order of the approximation is h^2 while after the simple transformation it becomes clear that the approximation is asymmetrical, in the case the approximation is only of order h!! The same is true for the time dependent equation.

Heat Conduction

Heat conduction follows exactly the law of diffusion. The difference is that we now follow the spreading of a heat impulse:

$$\vec{j}_T = -\lambda\nabla T$$

with λ the heat conductivity which may be once more a tensor. Concerning the energy balance (measured in J/s), however, this equation has to be related to the total energy change within a specific volume and that becomes

$$\frac{d}{dt}\iiint c\rho T dv,$$

with c the heat capacity and ρ the density of the material.

In a very careful consideration one has to observe that not just c and ρ are functions of the temperature but that the specific volume also depends on temperature. That means that the integral boundaries become a function of temperature, an effect usually ignored because for most solids the temperature dependent volume changes are rather small, however, that may not be true with certain metals or if we consider large amounts of solids as it is sometimes the case in geological problems. Here we will assume that the volume change can be ignored so that we can take the partial differential rather than the total (substantial) differential and the partial differential equation becomes

$$\frac{\partial c\rho T}{\partial t} = \nabla(\lambda\nabla T).$$

Observe that heat conduction occurs within the solid and the fluid. In principle we need two additional equations: $c = c(T)$ and $\rho = \rho(T)$, so that we arrive at a nonlinear problem unless one considers c and ρ to be constant (independent of Temperature), an assumption frequently applied in simple geological and geophysical models. For the dimensions of the parameters see the appendix to this chapter.

In large scale geological systems it becomes sometimes necessary to consider heat production within certain rock types due to radioactive decay or chemical processes which also may consume heat. Typical rocks producing heat are by example granites and claystones. In this case we have to consider the more general equation

$$\frac{\partial c\rho T}{\partial t} \pm Q = \nabla(\lambda \nabla T)$$

In the literature you will find frequently the equation

$c\rho \frac{\partial T}{\partial t} = \nabla(\lambda \nabla T)$, i.e. the 'temperature equation' which is only valid if $c\rho = const$ in which case the equation can be further simplified:

$$\frac{\partial T}{\partial t} = \nabla(D_T \nabla T), \quad D_T = \frac{\lambda}{c\rho}.$$

In porous media we have to consider an additional aspect: The medium consists of solids and of pores filled wit some fluid like water, oil or some gas (air). The ratio of the pores to the volume is defined by the porosity

$\varphi = \frac{porevolume}{bulkvolume}$, a dimensionless number (bulk-volume=total volume).

In detail then we have to consider the composition of the porous medium and the parameters become

$$\rho = \rho_{bulk} = (1-\varphi)\rho_{solids} + \varphi\rho_{fluid}$$

$$c = c_{bulk} = (1-\varphi)c_{solids} + \varphi c_{fluid}$$

Thereby the solids may be further differentiated if their fractions f_i are known:

$$\rho_{solids} = \sum f_i \rho_i, \quad c_{solids} = \sum f_i c_i, \quad \sum f_i = 1$$

In a similar way the heat conductivity λ is split into two components, however, as it may be a tensor, the process is at best a first order approximation if it can be considered a scalar. The approximation sometimes used is the geometric mean or

$\overline{\lambda} = \lambda_{solid}^{1-\varphi} \lambda_{fluid}^{\phi}$, which obviously is less easily extended to a multi component system, to do it is a nice exercise.

Exercises

1) *Linearize the equation* $\frac{\partial c\rho T}{\partial t} = \nabla(\lambda \nabla T)$ *by partially differentiating the time derivative with respect to the parameters, observing that c=c(T) and* $\rho = \rho(T)$.

2) *Consider the heat flow from the interior of the earth which mostly is considered stationary, i.e. it is governed by the equation* $\nabla(\lambda \nabla T) = 0$ *or* $\nabla(\lambda \nabla T) = Q$. *At the surface an average thermal gradient of 30°C is observed. At about 100 km depth the boundary between the lithosphere and the astenosphere is reached, the latter behaves like a fluid due to seismological data, the temperature at this boundary is approximately 1300°C, due to experiments.*
    a) *Compute the expected temperature at the base of the lithosphere based on the average surface gradient.*
    b) *Compute the expected temperature gradient throughout the lithosphere, based on a surface temperature of 0°C.*
    c) *Discuss for a layered crust qualitatively how the thermal conductivity* λ *should vary with depth if the equation* $\nabla(\lambda \nabla T) = 0$ *holds. Compare your results with conductivity data for real rocks.*
    d) *Determine for a homogenous lithosphere the ratio of* Q / λ *required to match the observed boundary conditions.*

Fluid Flow in Porous Media

What's left is the fluid flow through a porous medium. Also this part may be considered and indeed may be the dominating process; the discussion has been shifted to the end because there is a lot of confusion and alternative approaches around in the literature. You may find essentially **three** different definitions which also affect the definition of permeability:

1) $\vec{q}_M = \frac{k\rho}{\mu}(\nabla p - \vec{g}\rho)$, the mass flow of the fluid [(kg m)/s],

2) $\vec{q}_D = K\nabla(p - g\bar{\rho}z)$, the Darcy velocity [m/s],

3) $\vec{q}_h = K^*\nabla(h)$ or $\vec{q}_h = K^*\frac{\Delta h}{\Delta l}$ or´ $\vec{q}_D = K\nabla(p/\gamma + z)$, as an alternative definition of the Darcy velocity [m/s].

The parameters and variables involved are:

ρ, the actual density at a certain point in space;

$\bar{\rho}$, the constant density at a constant temperature, ignoring the pressure dependence of the fluid (water close to zero);

γ, the unit weight of water [kp];

μ, the dynamic viscosity of the fluid which may also depend on temperature;

g, is the normalized acceleration on earth and

$\vec{g}$, the vector in the direction of acceleration (in small scale models it acts in the vertical (z) direction);

z, is the height of a water column as measured in a piezometer or a well,

p, is the pressure in the fluid [N/m^2];

k, K, K^*, have different dimensions although they formally describe the same property but with different assumptions concerning the variability of μ and ρ; k has the dimension [m^2], K is, especially in the oil industry, referred in [Darcy], and K^* has the dimension [m/s]. The different definitions and assumptions caused confusion very early and it is not easy to recalculate published permeability data between the different concepts. This is well illustrated by the facsimile at the end of this chapter from 'Theoretical Soil Mechanics' (John Wiley and Sons, Inc., 1943). Note that k, K are used differently in Terzaghi's notation (vice versa), here we follow the presently (mostly) accepted notation.

88. Flow of water through soils. The path along which a water particle travels through a mass of soil is called a *flow line*. If the flow lines are straight and parallel the flow is a *linear flow*. The flow of water in a downward direction through a horizontal bed of sand is an

example of this type. If the water particles travel along curves in parallel planes, the flow is two-dimensional. All other types of flow, such as the flow toward wells, are three-dimensional. In connection with foundation problems we are primarily interested in two-dimensional types of flow. The flow of water out of a storage reservoir through the soil located beneath the foundation of a dam belongs in this category.

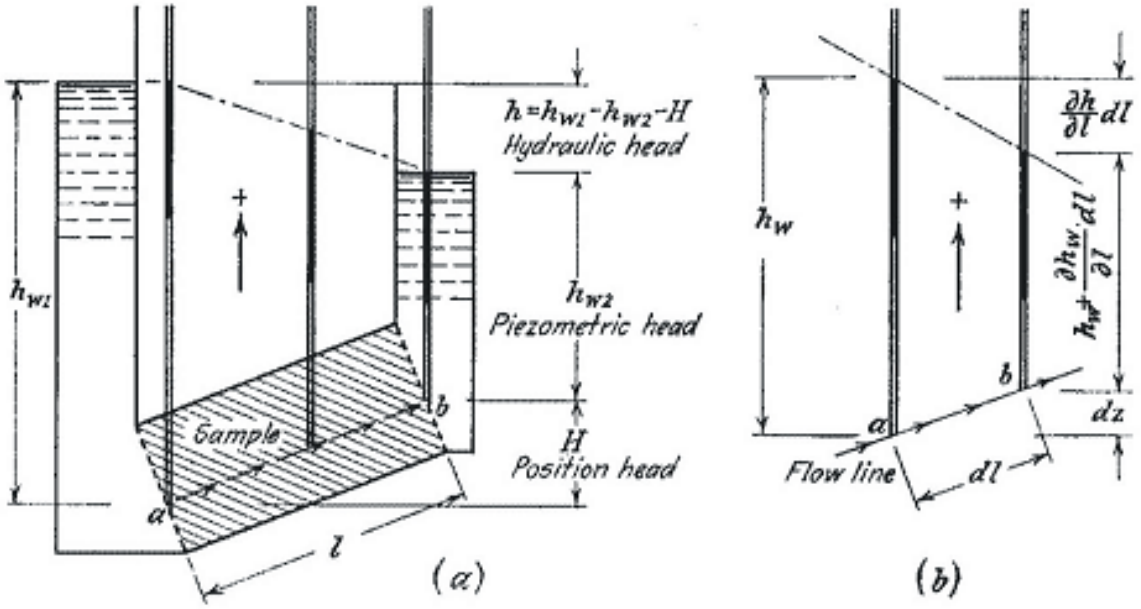

FIG. 72. Meaning of terms and symbols used in theory of seepage if used in connection with (*a*) linear flow and (*b*) two- or three-dimensional flow involving curved flow lines of which *dl* is an element.

Figure 72*a* is a section through one of several types of an apparatus which could be used to establish a linear flow in a soil sample with finite dimensions. The sample is contained in a prismatic box with a length l and a cross-sectional area A. The sides of the box are impermeable. The two ends are perforated to permit free communication between the soil and the adjoining columns of free water. The line ab represents one of the flow lines. The neutral stress at point a is

$$u_{w1} = \gamma_w h_{w1} \qquad [1]$$

and at point b

$$u_{w2} = \gamma_w h_{w2} \qquad [2]$$

If the water stands at the same level in the two piezometric tubes at a and b the water is in a state of rest, although the neutral stresses u_{w1} and u_{w2} may be very different. In order to cause the water to flow through the sand it is necessary to establish a hydraulic head h (Fig. 72*a*) which increases the hydrostatic pressure in one tube by $\gamma_w h$ in excess of the hydrostatic pressure in the other tube at the same level.

This *excess hydrostatic pressure* $\gamma_w h$ represents the force which drives the water through the sand. The ratio

$$i_p = \gamma_w \frac{h}{l} \qquad [3]$$

represents the *pressure gradient* between the points a and b. It has the dimension of a unit weight, gm cm^{-3}. The ratio

$$i = \frac{i_p}{\gamma_w} = \frac{h}{l} \qquad [4]$$

is the *hydraulic gradient*. It is a pure number.

The quantity of water which percolates per unit of time through the unit of area of a section at right angles to the direction of the flow is called the *discharge velocity* v. For fine sands and for soils finer than sand the relation between the pressure gradient i_p, equation 3, and the corresponding discharge velocity v can be expressed almost exactly by the equation

$$v = \frac{K}{\eta} i_p \qquad [5]$$

wherein η (gm cm^{-2} sec) is the coefficient of viscosity of the liquid and K (cm^2) an empirical constant. The value η depends to a certain extent on the temperature of the liquid and the value K on the porosity and on the shape and size of the voids in the porous material. In physics the value K is called the coefficient of permeability. By combining equations 4 and 5 we get

$$v = \frac{K}{\eta} \gamma_w i$$

The only liquid with which the civil engineer has to deal in connection with seepage problems is water. Within the range of temperatures to be encountered under field conditions the values η (viscosity) and γ_w (unit weight) of water are almost constant. Therefore it is customary in civil engineering to assume that both values are constant and to substitute in the preceding equation the value

$$k = \frac{K}{\eta} \gamma_w \qquad [6]$$

whence

$$v = ki = k \frac{h}{l} \qquad [7]$$

The value k is also called the *coefficient of permeability*. However, in

contrast to the value K used by the physicists it has the dimension of a velocity, cm per sec. It represents the discharge velocity for a hydraulic gradient i equal to unity, and the law expressed by equation 7 is called *Darcy's law* (Darcy 1856). According to this law the quantity of water which flows per unit of time through the sample shown in Figure 72*a* is

$$q = Av = Aki$$

In connection with equation 6 it should be emphasized that the permeability characteristics of a porous material are expressed by K (cm^2) and not by k ($cm\ sec^{-1}$), because K is independent of the unit weight and the viscosity of the percolating liquid whereas k depends on these factors. The exclusive use of k in this book and in civil engineering in general is justified only by convenience.

Within the sample the water occupies only a volume n per unit of volume of the soil. Therefore the average velocity with which the water particles travel in a direction parallel to the flow lines is

$$v_s = \frac{1}{n} v \qquad [8]$$

which is called the *seepage velocity.*

From the data shown in Figure 72*a* we obtain the following relations. If h_{w1} and h_{w2} represent the piezometric heads at a and b respectively, the hydrostatic head h is equal to

$$h = h_{w1} - h_{w2} - H \qquad [9]$$

and the hydraulic gradient is

$$i = \frac{h}{l} = \frac{h_{w1} - h_{w2}}{l} - \frac{H}{l} \qquad [10]$$

Since $h_{w1} = u_{w1}/\gamma_w$ (eq. 1) and $h_{w2} = u_{w2}/\gamma_w$ (eq. 2), equation 10 can be replaced by

$$i = \frac{1}{\gamma_w} \frac{u_{w1} - u_{w2}}{l} - \frac{H}{l} \qquad [11]$$

If the flow occurs in a vertical direction, H in equations 10 and 11 is equal to l, whence

$$i = \frac{h_{w1} - h_{w2}}{H} - 1 = \frac{1}{\gamma_w} \frac{u_{w1} - u_{w2}}{H} - 1 \qquad [12]$$

A positive value of i indicates that the hydraulic gradient produces a flow in an upward direction.

In Figure 72*b* the line ab represents an element of an arbitrarily curved flow line. The length of the element is dl. At one end a of the element the water rises in a piezometric tube to a height h_w above a and at the other end b it rises to an elevation

$$h_w + \frac{\partial h_w}{\partial l} dl$$

The difference between the elevation of the observation points a and b is dz. Substituting in equation 10

$$l = dl, \quad \frac{h}{l} = -\frac{\partial h}{\partial l}, \quad h_{w1} = h_w, \quad h_{w2} = h_w + \frac{\partial h_w}{\partial l} dl$$

and

$$H = dz$$

we obtain

$$i = -\frac{\partial h}{\partial l} = -\frac{\partial h_w}{\partial l} - \frac{\partial z}{\partial l} \qquad [13]$$

Since

$$u_w = h_w \gamma_w \quad \text{or} \quad h_w = \frac{u_w}{\gamma_w} \quad \text{and} \quad \frac{\partial h_w}{\partial l} = \frac{1}{\gamma_w} \frac{\partial u_w}{\partial l}$$

we can also write

$$i = -\frac{1}{\gamma_w} \frac{\partial u_w}{\partial l} - \frac{\partial z}{\partial l} \qquad [14]$$

The pressure gradient is equal to

$$i_p = -\gamma_w \frac{\partial h}{\partial l} = \gamma_w i \qquad [15]$$

Concerning the different definitions for the fluid flux, $\vec{q}_M = \frac{k\rho}{\mu}(\nabla p - g\rho)$ is the most general one from which the other ones can be derived. By balancing with the changes in a certain volume the following differential equation for the mass of fluid is derived:

$$\frac{\partial \varphi\rho}{\partial t} \pm Q = \nabla(\frac{k\rho}{\mu}(\nabla p - \vec{g}\rho)),$$

which can only be solved together with the equation of state $\rho = \rho(p)$ or more general $\rho = \rho(p,T)$. Q is a source/sink term which in large scale geological systems can be related to the alteration of minerals which under certain conditions release or bind water.

Assuming $\varphi = const$, Q=0, and $\rho = \rho(p)$ the equation can be linearized by partial differentiation:

$$\varphi \frac{\partial \rho}{\partial p}\frac{\partial p}{\partial t} = \nabla(\frac{k\rho}{\mu}(\nabla p - \vec{g}\rho)).$$

Considering $\frac{\partial \rho}{\partial p} = const$ we get

$$\varphi c_f \frac{\partial p}{\partial t} = \nabla(\frac{k\rho}{\mu}(\nabla p - \vec{g}\rho)),$$

a linear equation which only depends on p, c_f is the compressibility of the fluid .

Assuming further that $\rho = \bar{\rho} = const$ and $p = \bar{g}\bar{\rho}h$ we find from the last equation

$$\varphi c_f \frac{\partial h}{\partial t} = \nabla(\frac{k}{g\mu}\nabla(h)),$$

which is sometimes found in the literature. However, here the dog is biting in its tail because previously we only assumed $\frac{\partial \rho}{\partial p} = const$, now we are actually assuming that $\rho = const$, in which case the original equation becomes

$$0 = \nabla(\frac{k}{g\mu}\nabla(h)) \text{ or } 0 = \nabla(K^*\nabla(h)),$$

i.e. the time dependent problem reduces to a pure stationary one, which has been of importance before the invention of digital computers because it was possible to solve this equation analytically for simplified models or by using analog computers in the 50th and 60th of the 20th century, using the black box analogy with electrostatics. The discrepancy, however, only occurs if we consider the three dimensional case or a confined aquifer. If, in case of an unconfined aquifer, the problem is reduced to two dimensions (x,y) and the third dimension (z) becomes the dependent variable in terms of the hydraulic head h, then an equation of the type

$$S\frac{\partial h}{\partial t} = \nabla(\frac{k}{g\mu}\nabla(h))$$

results, with S the storage capacity which is $S = \varphi c_f h$.

There are some more approaches available to relate h and $\nabla p - \vec{g}\rho$, which are more concise, however this will be explained in the context of FEFLOW®.

REMARK
Darcy's law is valid as long as the flow through the porous medium is governed by capillary forces, even if very narrow joints are involved. However, as soon as the connections within the porous medium approach pipe size like sometimes in coarse gravel or in open joints this basic approach fails. In this case other laws have been developed e.g. the

Forchheimer equation: $a\vec{q} + b\vec{q}^2 = \nabla(K(\nabla p - \vec{g}\rho))$

Or potential functions : $c\vec{q}^n = \nabla(K(\nabla p - \vec{g}\rho))$.

In addition a **dispersion** term is sometimes introduced which considers that the pore network provides a net with complex interactions causing a lateral dispersion of the flow. However, this term is hardly determined experimentally in large scale systems, and it should depend on the flow velocity, going to zero as the flow goes to zero or it may approach the diffusion coefficient in case solutes are involved.

Dimensions occurring in the equations

The classical literature is confused by a variety of different units which have been in use in the past. Here some relationships are summarized.

Joule: work=*Force X Distance, 1 J = 1 N m = 1m^2 kg s^{-2} =1 W s*
1 J = 10^7 erg=10^7 dyn cm = 10^7 cm^2 g s^{-2}
1 cal =4.1855 J
Watt: *1 W = 10^7 erg/s=(10^7 cm^2 g)/s^2 =1J/s=1 m N/s*
Newton [N]: N= $mass \times acceleration$, 1 N=1 m kg s^{-2}
1 N=10^5 dyn=10^5 cm g s^{-2} =0.1019716 kp
Pressure, Pascal [Pa]: *pressure=force/area,*
*1 Pa=1 N m^{-2} = 10^{-5} bar=0.101972 kp m^{-2} =0.98693*10^{-5} atm*
Velocity: *[m s^{-1}]*
Mass flux: *[kg m s^{-1}]*
Mass [ρ]: *[kg m^{-3}]*
Porosity [φ *],* sometimes *[n]***:** *Volume of pore space/ Bulk volume [dimensionless]*
Permeability, intrinsic [k]: *[m^2]*
Permeabilty, Darcy [K]: *((dynamic viscosity)/(pressure difference)) X ((flow rate)/area))*
*1 D=(10^{-2} dyn s/cm^2)/(1 atm/cm) * (1 cm^2 /s)/(1 cm^2)= 0.987*10^{-8} cm^2*
Permeability, hydrostatic [K*]*: [m/s]*
Heat conduction [λ]**:** *1 J/(s m °K)*
Specific Heat, [c]:*1 J/(°C kg) = 1 J/(°K kg)= 10^4 cm/(s^2 °K)*
Heat production: *W=J/s, mostly given as* μW
Dynamic Viscosity: *10 g/(cm s)=1 kg/(m s)=(0.102 kp s) /m^2*

Coupled Mass and Energy Transport

In the last chapter we considered the transport equation for mass, heat, and fluid transport and already observed that they are not independent concerning the state variables involved. However, in addition we have to consider that the moving fluid may transport excessive mass as well as heat, both modifying the associated properties and in addition may modify the state parameters like ρ, λ, c, μ. Returning to the considerations of chapter 2, the fluid flow provides an external vector field or flow field modifying the content of the control volume despite any additional complications like chemical reactions. It is left to you to verify the following equations by using the machinery developed in chapter 2.

The conservation of mass becomes

1) $\frac{\partial \varphi C}{\partial t} - \nabla(D(\nabla C)) + \nabla(C\vec{q}) + Q_C = 0$.

Similar we get for the heat transport

2) $\frac{\partial c_b \rho_b T}{\partial t} - \nabla(\lambda(\nabla T)) + \nabla(c_f \rho_f T\vec{q}) + Q_T = 0$,

where the subscript b defines the bulk value (bulk density, bulk heat capacity, while the subscript *f* stays for the properties of the pore fluid. Equations relating the bulk properties with the fluid properties have been given above.

The pore water flow is given by

3) $\frac{\partial \varphi \rho_f}{\partial t} + \nabla\vec{q} + Q_f = 0$, $\vec{q} = -\frac{k\rho}{\mu}(\nabla p - \vec{g}\rho)$.

In order to solve this non linear set of equations we need additional information concerning the state variables:

$\varphi = \varphi(p, T, Q_c)$ usually is not considered, i.e. $\varphi = const$, otherwise additional equations, perhaps expressed as differential equations may be involved or in other words the basic consideration concerning a stationary volume will be violated, as previously has been discussed for the thermal expansion/contraction.

D=D(T) provides a good approximation, similarly

$c_b = c_b(p, T, Q_c)$, $c_f = c_f(p, T, Q_c)$ are normally reduced to a pure temperature dependence,

λ is mostly considered constant, also it varies with p an T and, of course with the composition of the fluid!´

k is also mostly considered constant, although it strongly depends on the consolidation state of the rocks, including mechanical compaction and chemical reactions.

Mechanical compaction once more violates the way the differential equations have been derived because the control volume will change through time.

$\rho_f = \rho_f(p,T,Q_f)$ as well as $\rho_b = \rho_b(p,T,Q_f,Q_c)$, however, may have to be considered at least as $\rho_i = \rho_i(p,T)$ in the case of large scale geological models involving a wide variety of pressure and temperature values or if the 'fluid' is compressible, like in the case of a gas.

Q_i the various source/sink terms require additional assumptions like radioactive heat production, chemical reactions etc.

fluid and bulk properties are related by equations like

$$\rho = \rho_{bulk} = (1-\varphi)\rho_{solids} + \varphi\rho_{fluid}$$

$$c = c_{bulk} = (1-\varphi)c_{solids} + \varphi c_{fluid}$$

as discussed previously. They may generalized further as discussed above.

Considering all the aspects we approach slowly the real world. However, at the end we have an extremely high non-linear system which hardly can be solved with regard to the available algorithms and computer power, at least within the lifetime of a scientist. Any practical application, therefore will require simplified assumptions which focus at the major processes.

Recommended Exercise

Try to linearize equations (1) to (3) with regard to the time dependent state variables by ignoring possible source/sink terms (use partial differentiation).

Mathematical formulation of the thermohaline flow problem in FEFLOW

In the previous paragraphs, different constitutive equations describing mass, heat and fluid flow are given in the form of linear relationships between fluxes and driving forces (gradients). We already observed that those equations are not independent concerning the state variables involved. As additional remark, we should point out that forces of one type can generate flows of another type (Bear, 1988). By example, mass flux can be caused by temperature gradient (Soret effect) in addition to the concentration gradient (Fick's law) or, in the opposite case, concentration gradient can induce heat flow (Dufour effect), in addition to the temperature gradient. (Fourier's law). In this course, these cross-effects are neglected. We will rather assume that groundwater is driven by the gradient of $(p+\rho_f gz)$, appearing in the Darcy's law, as explained in the.

In nature, depending on the characteristics of the basin (e.g. presence of minerals and/or heat source), the "combination" of all or some of the previously described driving forces determines the quantity of $(p+\rho_f gz)$ and therefore the actual hydrologic regime of the basin. In other words, the synergy between the different processes is referred to as coupling. If in some regions the fluid density is greater than in the underlying units, the less dense fluids will tend to rise inducing convective currents. The archetypal example is the coupling of heat and dissolved halite which both strongly affect fluid density variation. The flow is then called thermohaline convection (Nield and Bejan 1999).

Here the mathematical formulation of coupled transport processes is given according to the notation used in FEFLOW.

$$S_0 \frac{\partial \varphi}{\partial t} + div(\mathbf{q}) = Q_{Boussinesq} \qquad \text{Eq. 1.1}$$

$$\mathbf{q} = -\mathbf{K}\left(\mathbf{grad}(\varphi) + \frac{\rho_f - \rho_{0f}}{\rho_{0f}} \mathbf{u} \right) \qquad \text{Eq. 1.2}$$

$$\frac{\partial \phi C}{\partial t} + div(\mathbf{q}C) - div\left(\mathbf{D}\mathbf{grad}(C)\right) = Q_C \qquad \text{Eq. 1.3}$$

$$\frac{\partial}{\partial t}\left(\left(\phi \rho_f c_f + (1-\phi)\rho_s c_s \right) + div(\rho_f c_f T\mathbf{q}) - div\left(\boldsymbol{\lambda}\mathbf{grad}(T)\right) = Q_T \right) \qquad \text{Eq. 1.4}$$

Eq. 1.1 is the equation of fluid mass conservation. S_0 is the medium storativity which physically represents the volume of water released (or added to) from storage in the aquifer per unit volume of aquifer and per unit decline (or rise) of head φ. $Q_{Boussinesq}$ is the Boussinesq term which incorporates first order derivatives of mass-dependent and temperature dependent compression effects. **q** is the Darcy (or volumetric flux density velocity) defining the specific discharge of the fluid. The Darcy's law is expressed by Eq. 1.2 where **K** is the hydraulic conductivity tensor. Eq. 1.3 is the equation of solute mass conservation where ϕ is the porosity of the porous medium, C is the mass concentration, **D** is the tensor of hydrodynamic dispersion and Q_c is a mass supply. Eq. 1.4 is the energy balance equation of the fluid and porous media. c_f and c_s is the heat capacity of the fluid and solid respectively, T is the temperature, $\boldsymbol{\lambda}$ is the tensor of hydrodynamic thermodispersion.

Constitutive and phenomenological relations of the different physical parameters involved in the equations are needed to close this coupled system. Here the hydraulic conductivity relation and the Equation of State (EOS) for the fluid density are recalled:

$$\mathbf{K} = \frac{\mathbf{k}\rho_{0f} g}{\mu_f(C,T)} \qquad \text{Eq. 1.5}$$

$$\rho_f = \rho_{0f}\left(1-\beta(T,p)(T-T_0)+\gamma(T,p)(p-p_0)+\frac{\alpha}{C_s-C_0}(C-C_0)\right) \qquad \text{Eq. 1.6}$$

The hydraulic conductivity tensor **K** is related to the reference fluid density ρ_{0f}, g is the gravitational acceleration, **k** is the tensor of permeability, $\mu_f(C,T)$ takes into account the fluid viscosity effects due to temperature and concentration variations. The EOS for the fluid density Eq. 1.6 is related to the reference temperature T_0, pressure p_0 and concentration C_0. α is the mass concentration ratio, $\beta(T,p)$ is the coefficient of thermal expansion and $\gamma(T,p)$ is the coefficient of compressibility.

As previously, mentioned the primary coupling between groundwater flow, mass and heat transport processes is through the Darcy law. The Darcy flow rate **q** in Eq. 1.2 controls the rate of heat and mass convected through the media (equations 1.3 and 1.4) and is also a function of fluid density and dynamic viscosity, which are both related on temperature, solute concentration and pressure by the respective EOS.

Therefore coupled fluid flow processes are intrinsically controlled by (1) the hydraulic permeability distribution and (2) fluid properties appearing in the Darcy law. In other words, the interplay of both solid and fluid properties determines the distribution of fluid pressure, flow rates, heat and solute migration.

1. Since sedimentation processes occurred over geological time-scale, hydraulic conductivity can exhibit a wide range of values in the vertical direction. The heterogeinity of hydraulic conductivity is also evident in the surroundings of piercing salt domes (quasi-impervious), Pleistocene channels (highly permeable) and faults (permeable/impervious depending on the core properties). For instance, in-situ measured permeability data in fractured crystalline rocks can display variations of several orders of magnitude (Ingebristen and Sanford, 1998). Furthermore compositionally identical rocks can have different permeability at different depths because of consolidation and temperature effects. An example of the relative importance of hydraulic permeability in controlling coupled processes is faulted systems is given for the western Anatolia example.

2. The major fluid properties coupling fluid flow processes are density and viscosity. On one hand, density variations must be accounted in the Darcy formulation to correctly calculate buoyant driving forces, in addition to the pressure gradient (Eq. 1.2). Only very small concentration differences are required to achieve density driven flow gradients equivalent to typical field scale hydraulic head gradients (Simmons, 2005). On the other hand, as fluid viscosity appears in the denominator of the hydraulic conductivity formula (Eq. 1.5), small viscosity variations will highly impact the effective hydraulic conductivity and consequently the flow rates. EOS are needed to correctly describe temperature, pressure and concentration dependences of density (Eq. 1.6) and viscosity. As fluid properties strongly depend on temperature and concentration, any effect which causes a significant variation in temperature and concentration will play a fundamental role in controlling groundwater flow. In sedimentary basins, salt diapirs strongly influence the concentration of dissolved solids. Furthermore, salt diapirs also perturb the temperature field because of their high thermal conductivity which is two to four times greater than that of the surrounding sediments. In this regard, one can say that salt diapirs are a unique geological environment controlling

thermohaline flow. Near salt domes, the impact of fluid viscosity is twofold: In a colder and highly saline environment, such as a shallow salt-dome crest, it retards brine flow by decreasing the effective hydraulic conductivity. In a warmer and less saline environment, variable fluid viscosity enhances thermally induced flow. The coupling of transport processes will be illustrated for the salt domes of the North East German Basin (NEGB).

A key number which controls the flow dynamics is the Rayleigh number. If the Rayleigh number is large enough, then cellular motion can develop. As a result, a multitude of stability analyses based on laboratory experiments were carried out on saturated porous media with vertical gradients of temperature and salinity in order to determine the critical Rayleigh number for the onset of thermohaline convection (Horton and Rogers 1945; Lapwood 1948; Elder 1967).

Stability criteria

A dimensional analysis of the governing balance equations (Eq.(1.1) to Eq.(1.4)) yield to the definition of the several adimensional numbers (Nield and Bejan 1999).

The key dimensionless number is the Rayleigh number (*Ra*), which is the ratio between buoyancy-driven forces and resisting forces caused by diffusion and dispersion:

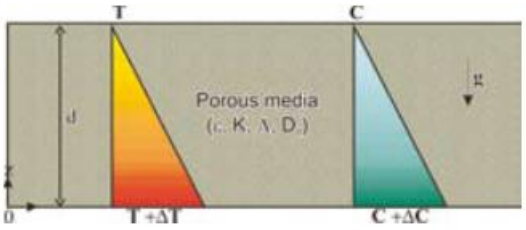

Schematic temperature and concentration profiles of a homogeneous porous layer heated from below. Given thephysical properties of the medium, the Rayleigh numbers can be determined (Eq.1.7 and Eq.1.8).

<u>*Thermal Rayleigh number*</u> Ra_t

$$Ra_T = \frac{K\bar{\beta}\Delta T d}{\Lambda} \tag{1.7}$$

<u>Solutal Rayleigh number</u> Ra_s

$$Ra_s = \frac{\frac{\bar{\alpha}}{C_{sat} - C_0} K \Delta C d}{\varepsilon D_d} \tag{1.8}$$

where K is the hydraulic conductivity as defined in Eq.(1.5) $\bar{\alpha}$ introduces the effect of a density change due to the concentration the solute at temperature and pressure $\bar{\beta}$ is the coefficient of thermal expansion at constant pressure and concentration, Λ is the thermal diffusivity, ΔC and ΔT are respectively the concentration and temperature variation, d is a characteristic length of the porous media (e.g., the layer thickness), ε is the porosity, D_d is the coefficient of molecular diffusion.

The solutal and thermal Rayleigh numbers are related by:

$$Ra_s = N \times Le \times Ra_T \tag{1.9}$$

where the dimensionless numbers in connection with heat and mass transport are:

<u>*Buoyancy ratio (Turner)*</u> N is the relative effects of concentration and temperature on controlling groundwater density

$$N = \frac{\frac{\bar{\alpha}}{C_{sat} - C_0} \Delta C}{\bar{\beta} \Delta T} \tag{1.10}$$

<u>*Lewis number*</u> Le is the ratio of thermal to mass diffusivity

$$Le = \frac{\Lambda}{\varepsilon D_d} \tag{1.11}$$

The stability criteria is thoroughly explained in Nield (1991), Diersch and Kolditz (2002). Here the main points are recalled.

- The monotonic instability (or stationary convection) boundary is a straight line defined by $Ra_C = Ra_T + Ra_s = 4\pi^2$, where Ra_C is the critical Rayleigh number. The critical Rayleigh number defines the transition between dispersive/diffusive solute transport ($Ra < Ra_C$) and convective transport by density-driven fingers ($Ra > Ra_C$). Ra_C depends on the boundary conditions, geometry and anisotropy (Nield 1968).

- The region delimited by $Ra_T + Ra_s < 4\pi^2$ is a stable regime characterized by pure conduction and no convection.
- In a range between $4\pi^2 < Ra_T + Ra_s < 240-300$ steady state convective cells develop as two-dimensional rolls rotating in clockwise or counter-clockwise direction. A second critical Rayleigh number $Ra_{c2} = 240-300$ is identified as an upper limit.
- For $Ra_T + Ra_s > Ra_{c2}$ the convection regime is unstable and characterized by a transition to an oscillatory and transient convection behaviour.

From Eq.(1.7) and Eq.(1.8), it can be seen that given the diffusivities of the unit, Rayleigh numbers are directly proportional to units thickness and hydraulic conductivity. Therefore convective flows (i.e. high Rayleigh numbers) likely occur within thicker and more permeable layers.

Brief description of driving forces in large-scale groundwater flow systems

In sedimentary basins, different driving forces contribute to the transfer of mass and heat. These are often referred to as *hydrogeologic regimes*. Flow, transport and reaction at the scale of sedimentary basins are in most cases slow processes. However, over the scale of geologic time, they effects are of great importance as they can generate important energy resources.

Topography driven flow (forced convection) (Fig. 1.3) is the dominant regional-scale groundwater flow in uplifted sedimentary basins, both in the shallow and deep sub-surface (Freeze et al., 1967).

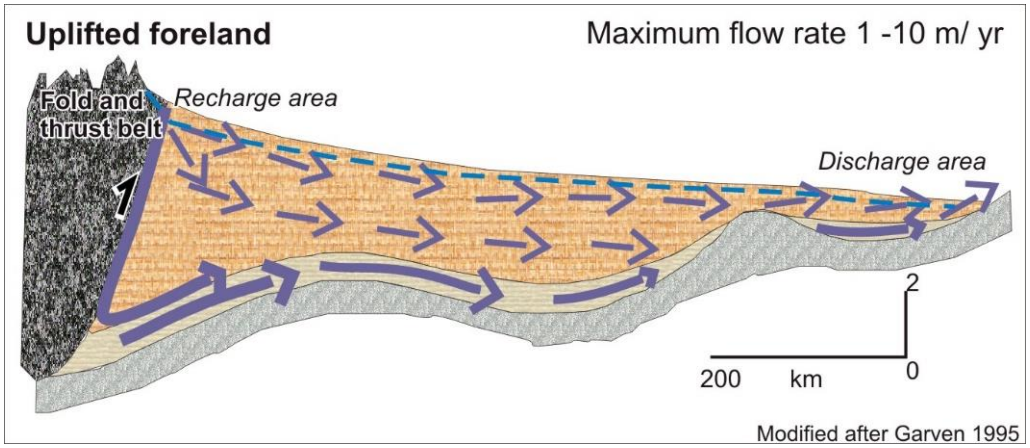

Fig. 1.3: *Topography driven flow* (forced convection) in an uplifted sedimentary basin. The dashed line illustrates the water-table that is a replica of the landscape. Vectors indicate the flow field. Stronger flow (thicker vector) occurs in more permeable units (m/yr: meter per year).

Usually, in a foreland basin the water table mimics the topographic relief (blue dashed lines in Fig. 1.3). A regional flow is induced because of the differences in the hydrostatic head that drive fluid from high-elevation recharge areas to low-elevation discharge areas. In general, groundwater flow is called *forced convection* when it is driven by water table gradients.
Flow lines (bold vectors in Fig. 1.3) and rates depend on several factors as the geometry of the aquifers (e.g variable thickness) and their physical properties (e.g., hydraulic permeability). For instance, vigorous recharge flow can be observed within the fault as well as in the adjacent thin and highly permeable sand unit. Pleistocene channels (not displayed in Fig. 1.3) are also important geological features that strongly impact the velocity field and flow patterns. Almost no flow occurs in the bottom unit (e.g. impervious clay). Accordingly, typical maximum flow rates can strongly vary, ranging from 1 to 10 m year^{-1}.

Thermally driven flow (free convection). In sedimentary basins, the presence of a geothermal field induces fluid-density variations which in turn drive groundwater flow. Fluid motion caused by density difference due to temperature variations is called *free convection* (Fig. 1.4).

Most commonly, heating of groundwater in a geothermal system is provided by a heat source located at depths. In a porous media heated from below, the warmer fluid (i.e. less dense) starts to ascend. During this upward migration, the fluid loses its heat. Therefore buoyancy forces weaken and the fluid starts to sink again. The resulting flow path is called convective cell. Convective patterns are mainly controlled by the hydraulic permeability and the thickness of the units. Stronger convective flows are expected to take place in thick and permeable stratigraphic units whereas thin aquitards prevent the formation of any free convective motion. In highly permeable faults, a multi-cellular regime can develop and drive hot fluids to shallow depths. In the surroundings of faults, pressure and temperature patterns are strongly perturbed and differ from linear hydrostatic and conductive regimes. The impact of faults and less permeable units on geothermal energy migration is illustrated for the Western Anatolia example.

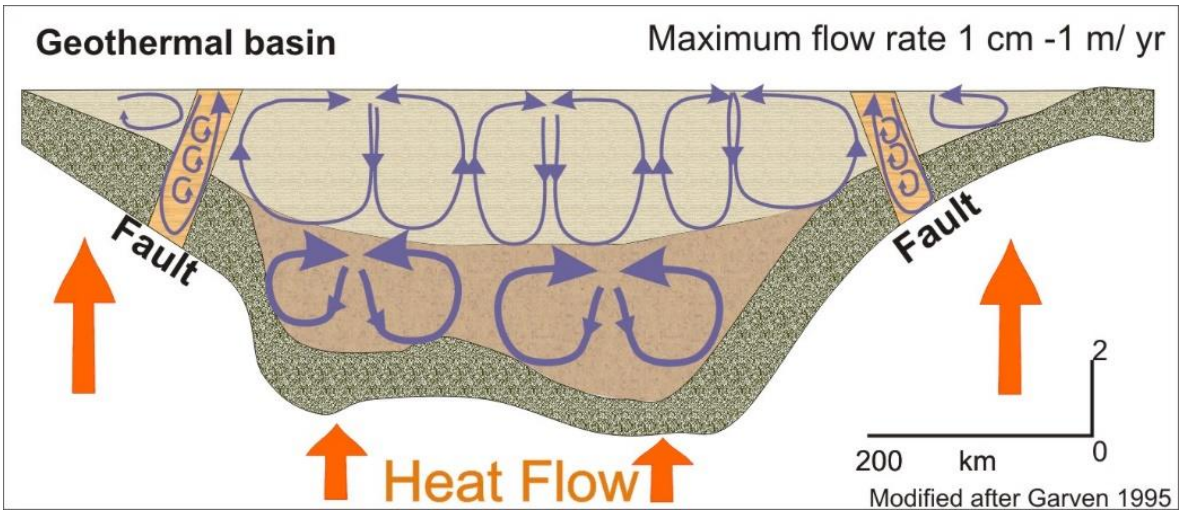

Fig. 1.4: *Thermally driven flow (free convection)* in a geothermal basin. Vectors illustrate the convective cells. Stronger convective flow (thicker vector) occurs in more permeable units. Near the faults, cells pattern are elongated toward the faults indicating that these units act as preferential pathways for fluid migration. (m/yr: meter per year).

In this regard, dimensionless studies based on Rayleigh and Prandtl numbers, as well as the evaluation of the buoyancy ratio, have been developed to determine the onset of convection in systems having a given thickness and constant physical parameters (Nield, 1968). However, in sedimentary basins, these conditions rarely, if ever, occur. Therefore, determining the onset of thermal convection by dimensionless analysis of the basin system is often not practical (Simmons et al., 2001). Flow rates in convection cells may vary from few centimeters per year up to a meter per year.

Gravity driven flow (or density driven flow) is the term used when the convective currents are induced by density differences due to variations of solute concentration. A favorable scenario for gravitational convection is the presence of large salt bodies extending into shallow units (Fig. 1.5). The formation of dense brines by dissolution at the base of these salt sheets destabilizes the hydrostatic equilibrium within the underlying sediments.

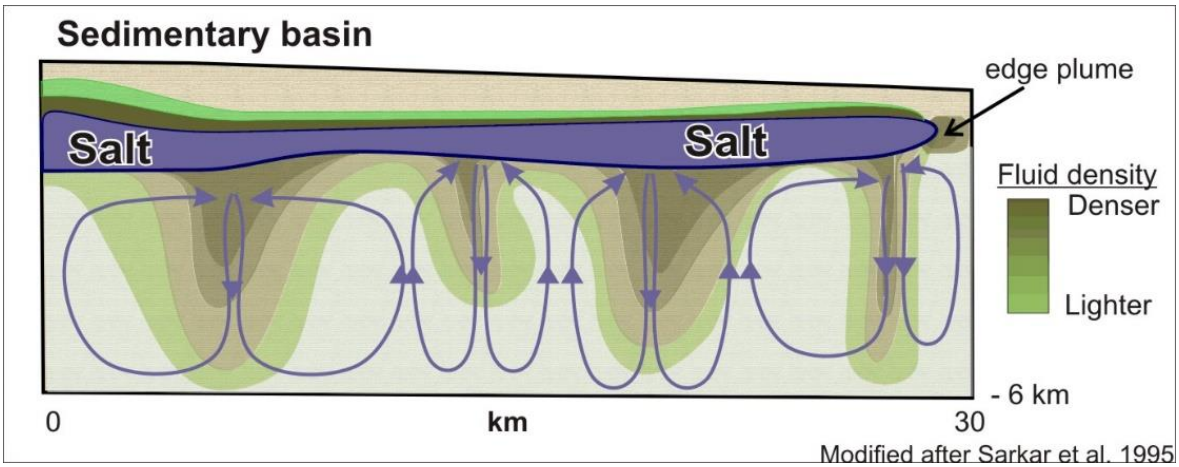

Fig. 1.5: *Gravitational convection* in a geothermal basin. Vectors illustrate the convective cells. (m/yr: meter per year)

Gravity instability beneath the base of the salt sheet manifests itself in the form of several incipient downwelling plumes in addition to the edge plume (Fig. 1.5). The solute plumes descend toward the base of the underlying sedimentary sequence. The resulting horizontal density gradients between the plumes give rise to orderly *counter-rotating* convections cells. This phenomenon can also be observed along the flanks of deep seated salt domes. However, in this case, the geothermal gradient also plays a role in inducing density variations and new effects might arise. These effects will be explained later in paragraph 1.3.

Ongoing geological processes such as sediment compaction, hydrocarbon generation or degassing of magma can also generate significant fluid flow at different velocity rates. These hydrologic regimes, also called *geological forcing* (Neuzil, 1995), are not considered in this work. Compactionally driven pore-water flow rates are usually very slow, in the order of 10^{-6} to 10^{-3} m year^{-1}, while tectonic compression can induce flow rates of 0.5 m year^{-1} (Garven, 1995). A thorough review can be found in Garven (1995).

Although the above mentioned driving forces have been described separately, in nature large-scale processes often occur together so that they cannot be regarded independently.

Coupled processes

Over the large spatial scales encountered in sedimentary basins, temperature and solute concentration vary strongly and basin deformations are often substantial. Therefore the driving forces of groundwater flow can interact leading to new hydrologic regimes. Depending on the characteristics of the basin (e.g. heat source, presence of minerals, ongoing compaction), the "combination" of all or some of the previously described driving forces will determine the hydrological behavior of the basin. In other words, the synergy between the different processes is referred to as *coupling* (Tsang, 1991; Bedehoefat and Norton, 1990). As Chen et al. (1990, p. 104) notes," *Although we tend to think of a single process it often happens that a variety of processes are coupled so strongly that qualitatively new effects and system behaviors arise because of this coupling*"

Thermohaline convection: the coupling of density-driven flow: The archetypal example for sedimentary basins is the coupling of heat and dissolved halite by controlling fluid density: the resulting regime is then called *thermohaline convection* (Nield and Bejan 1999). Since in geothermal basins the temperature gradients increase with depth, heat acts as a destabilizing potential. Thermohaline convection can develop cells at rates approaching 1 m yr^{-1} (Evans and Nunn, 1989; Garven, 1995) which are strong enough to control temperature and concentration fields. Excellent examples of thermohaline convection in a salt dome environment are the Gulf of Mexico (Evans and Nunn, 1989) and the NEGB which will be

thoroughly described later. Two major scenarios for thermohaline convection to occur can be distinguished:

(1) Salt concentration increases with depth, as for instance in the surroundings of deep-seated salt structures (Fig. 1.6).

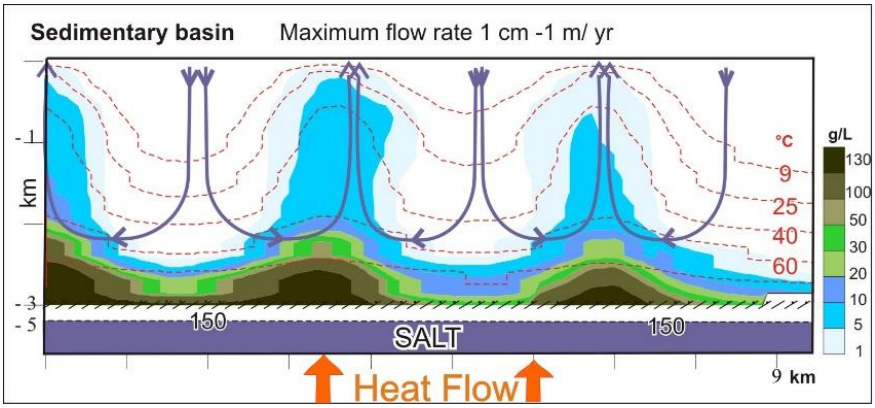

Fig. 1.6: *Thermohaline convection* above a deep salt structure, results from numerical simulations. Bold vectors illustrate the direction of the convective flow. The isotherms (red dashed lines) show typical convective multi-cellular regime. Picture modified after Magri et al. (2005). m/yr: meter per year

In this case, the salinity gradient acts as stabilizing force. The deeper brines are heated from below and become less dense: an upward flow will be triggered when thermal induced buoyant forces will overcome gravity, leading to the formation of salty plumes. As the plumes keep rising, the brines will cool off quickly while losing little salt because of the different rates of diffusion (heat diffuses faster than salt). Buoyancy forces will therefore weaken and brine will start sinking. The last part of this script provide examples of thermally driven flow around deep-seated salt domes.

(2) Another possible scenario arises when salinity gradients act as destabilizing factors. This can happen when brine forms in shallow areas of the basin (e.g., from shallow salt layers, Fig. 1.7). The denser fluid will therefore sink into the deeper sediments of the basin, depressing the isotherms. At the same time, lighter and hotter fluids will move upward owing to the thermally induced buoyant forces. Consequently, brine lenses and convection cells form.

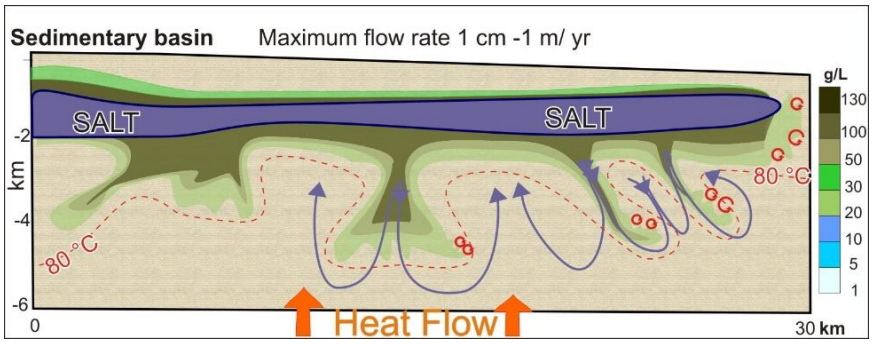

Fig. 1.7: *Gravitational convection* in a geothermal basin, results from numerical simulations. Bold vectors illustrate the direction of the convective flow. Smaller cells (red circles) can develop at the plume tips. Sinking brines decrease the temperature at depths (concave isotherms, red dashed lines). M/yr: meter per year

At the tips of both the sinking plumes and the edge plume, temperature oscillations can develop in a free-convective regime (red circles in Fig. 1.7), generating small brine fingers. This case is nicely illustrated for the Schleswig-Holstein shallow salt dome.

Mixed convection: the coupling of free and forced convection

When an external factor such as head-driven groundwater flow (forced convection) is imposed on a free thermohaline system the resulting regime is referred to as *mixed convection*. In sedimentary basins, it can happen that thermally-induced and topography-driven flows coexist (Raffensperger and Garven, 1995a; Thornton and Wilson, 2007). Under such mixed condition, the regional flow affects the shape of thermally induced flow patterns and brine plumes: the short wavelengths of the temperature oscillations and the elongated brine plumes characterizing the free thermohaline regime can merge in bigger cells (Fig. 1.8).

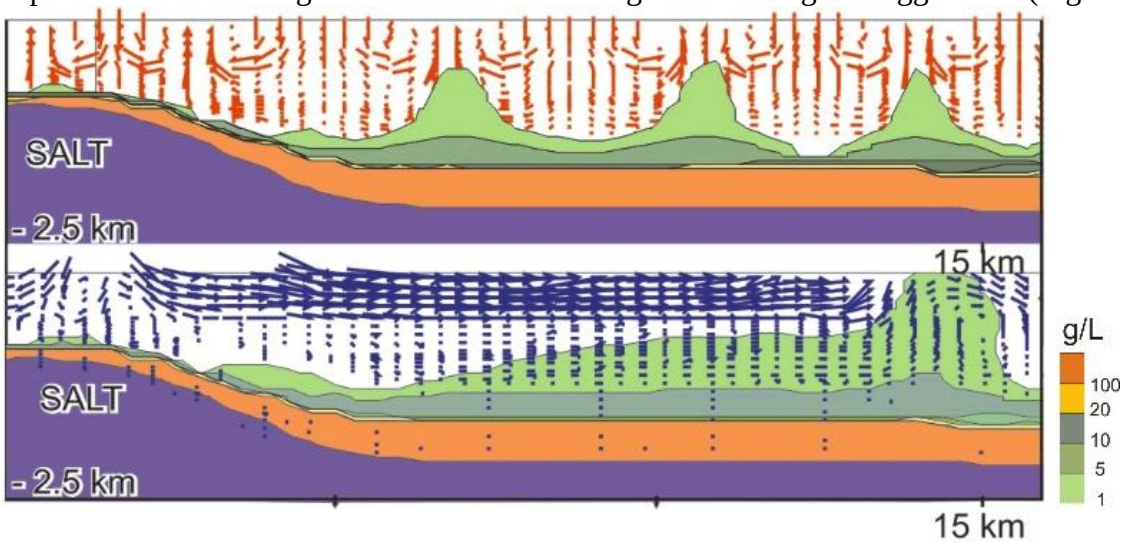

Fig. 1.8: *Mixed convection* near a salt dome, results from numerical simulations. Free thermohaline regime (top) compared to a mixed convective regime (bottom). The topography driven flow (blue vectors) overwhelms the thermohaline cells that would develop in a free regime (red vectors). In the mixed convective regime, only one larger brine finger reaches the surface. Modified after Magri et al. (2005)

On the other hand, vigorous topographically-driven groundwater flow can overwhelm free convection and modify the thermal structure of the basin. Precisely, it causes cooling and solute dilution in recharge areas whereas it increases heat flow and brine migration in discharge areas. In the NEGB (Chap 2), temperature and solute concentration differences can be observed between recharge and discharge areas reaching values of few degrees and few g/L, respectively. In active geothermal basins these differences can reach 50°C and several g/L (Ingebritsen and Sanford, 1998). An example of the strong impact of mixed convection on heat and solute transport is the Western Anatolia area (SBG example).

Other coupled processes

Additional effects that contribute to the coupling of hydrologic regimes have mechanical or chemical origins, such as dissolution or mineral precipitation that respectively increase or reduce both the porosity and permeability of rocks. These processes modify the spatial distribution of the physical properties and accordingly boost dramatically the complexity of the coupling effects. Hydromechanical and reactive transport coupling at basin-scale is the state of the art of numerical and mathematical studies, and require further research.

However, in a basin system the dominant hydrologic regime is the result of a complex interplay between the relative strength of the existing driving forces and other controlling factors. As it will be explained in paragraph 1.4, these controlling factors are related to the spatial distribution of the rock properties (e.g. hydraulic conductivity) and the fluid properties (density and viscosity

The Examples

The mathematical models given in previously can represent coupled transport processes at very slow rates. The rapidly increasing computer power and the development of user-friendly modeling software allows nowadays to solve those strongly coupled differential equations for systems which extend laterally for hundreds of kilometres and to depth of several kilometres over geologic time periods (i.e. thousands to millions of years). This length scale is henceforth referred to as large scale or sedimentary basin scale.

In the last two decades, numerical modeling has been applied to study the transient behaviour of temperature and mineral migration in sedimentary basins and to elucidate the controlling role of hydraulic permeability distributions. The most recent examples are numerical simulations of mid-ocean ridge hydrothermal systems (Ingebritsen et al., 2009).

Large scale simulation of coupled fluid flow, mass and heat transport based on a real geothermal system requires a proper fluid model and aquifers representation. EOS (e.g. Eq. 1.6) are used to reproduce the physical characteristics of fluid density and viscosity. The aquifer model should include the structural characteristics of the aquifers as well as the physical parameters such as porosities, hydraulic permeabilities, heat conductivity and heat capacity. For this purpose, the basin is usually divided in hydrostratigraphic units to represent hydraulically similar rock units (Bitzer et al., 2001). Because of the difficulty in representing the spatial and temporal variations of these properties, the general approach is to give an average or equivalent value of the physical rock properties to each hydrostratigraphic units. Therefore, the critical issues of basin-scale modeling are the accuracy of the hydrogeologic model and the correct evaluation of the associated equivalent properties. Several techniques exist to estimate equivalent hydraulic conductivity as summarized in Zhang et al. (2006). Here, the classical approach of representing the sedimentary deposits by a series of homogeneous hydrogeologic units is used. In this regard, the spatial discretization of the different units plays a crucial role in determining the accuracy of the numerical solution.

In the next two parts, the North East German Basin (NEGB) and the Seferihisar-Balçova Geothermal (SBG) area, Western Anatolia, serve as real study case examples whereby numerical models built with FEFLOW are applied to investigate hypotheses of (i) brine migration near salt domes (NEGB) and (ii) geothermal activity within faulted systems (SBG). In the NEGB case, heat and brine patterns are illustrated for a deep and shallow salt diaper. The impact of highly permeable faults in affecting coupled processes is investigated for the Western Anatolia case.

The North East German Basin (NEGB) example

In some areas of the NEGB, groundwater is anomalously salty. This is witnessed by the presence of several saline springs. Further evidence of saline waters is given by plants commonly found along sea beaches or in salty soils, such as seashore salt grass, which grow in different areas of the basin. Figure 2.7.1 illustrates two species of these plants (Sea Milkwort, Strand-Milchkraut and Sea Arrowgrass, Strand-Dreizack) found in Gröben, 50 km south of Berlin, during a field trip in 2004.

Fig. 1.9: Sea Milkwort, Strand-Milchkraut and Sea Arrowgrass, Strand-Dreizack in the Gröben area, 50 km south of Berlin.

The spontaneous growth of seashore grass far from the Baltic Sea coast is unusual and signals the existence of highly salty soils in the inner part of the basin.

Although these phenomena are observed since two centuries, the origin and mechanisms driving salt in the NEGB aquifer are not fully understood. A DFG funded research (2002-2008) allowed to carry out hydrochemical analyses of several spring and water samples from deep boreholes throughout the area. The results indicate that the main source of salinization is dissolution of evaporites at different depths. Therefore driving forces must exist to allow the deep-seated heavy brines to migrate and reach the surface.

As explained previously, salt structures are a unique geological environment controlling thermohaline flow, i.e. the coupling of heat and brine transport processes. Numerical models of coupled fluid flow in both deep and shallow salt structures of the NEGB are applied in order to investigate the role of the different forces and the controlling factors of brine migration in salt dome environment. The major outcomes are summarized here. The reader can refer to the publications within the DFG project for further details.

The incorporated geological data are derived from a three-dimensional structural model of the NEGB (Scheck 1997; Scheck and Bayer 1999). The area covered by the model is approximately 230 x 330 km across and 5 km in depth, consisting of 9 layers of sedimentary fill, including the basement. Figure 1.10 illustrates the geological structures of a representative cross-section. The NEGB is affected by intense salt tectonics. Thick salt diapirs pierce more than 4 km of overlying Mesozoic and Cenozoic strata. Salt crests can also be found 500 m below the surface level. Therefore, depth and thickness of sediment sequences vary greatly within the basin. The physical properties considered within each layer are constant. This first rough aquifer model differentiates only the stratigraphic layers of the model without any spatial variation in the horizontal direction. More details concerning the physical parameters of the sedimentary layers can be found in Magri et al. (2005).

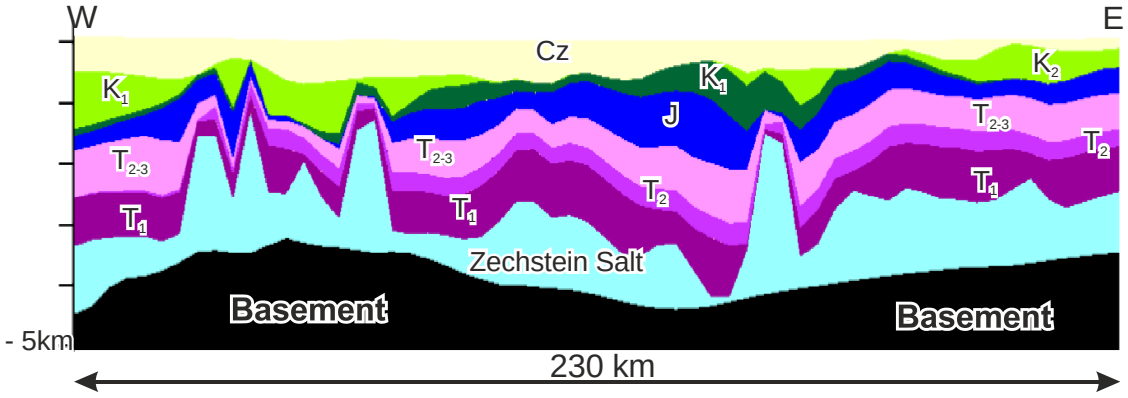

Fig. 1.10: Stratigraphic units of the 2D cross-section. This is the profile implemented into FEFLOW to carry out simulations of fully coupled fluid transport processes. The stratigraphic unit abbreviations are: Cz Cenozoic; K1 Upper Cretaceous; K2 Lower Cretaceous; J Jurassic; T2-3 Upper Triassic; T2 Middle Triassic; Lower Triassic; T1 Buntsandstein

With regard to the fluid model, brines are considered pure NaCl solution resulting from halite dissolution. The saturation concentration of the fluid on the top Zechstein is 345 g/L of dissolved halite, which corresponds to a brine density of 1220 g/L.

The simulations are run over the 2D cross-section illustrated in figure 1.10.

Figure 1.11(AB) shows the calculated temperature and concentration. The major result is that a disturbed temperature profile develops throughout the sediment fill above the Zechstein unit. The oscillatory pattern is characteristic of a multicellular convective regime. Below the

Zechstein unit the temperature profile is conductive everywhere, showing the well-known thermal anomalies within the salt diapirs (i.e., concave temperature isopleths).

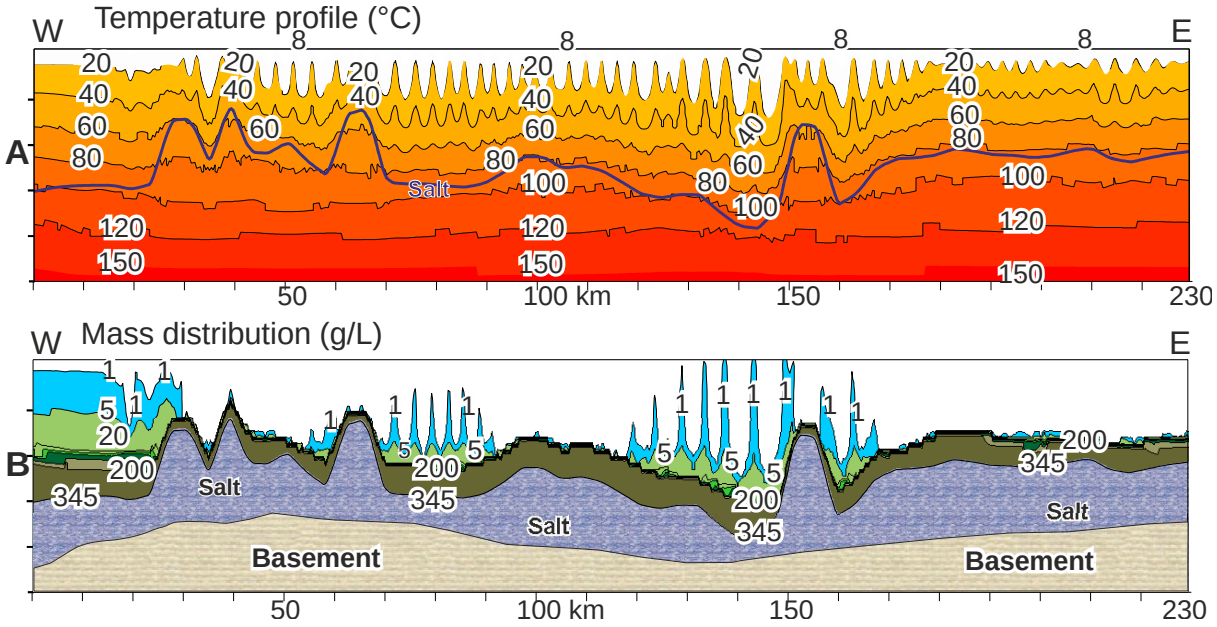

Fig. 1.11: A: temperature profile (°C) and B: Concentration (g/L) resulting from transient free thermohaline convection

The simulations suggest that the temperature oscillations can induce density variation strong enough to lift plumes of dissolved halite (Fig. 1.11 B). Above the Muschelkalk, brine plumes develop rapidly and penetrate the overburden (Fig. 1.11 B). Brine fingers form and extend vertically over 3 km throughout the sediments. At the eastern ending of the profile, brine plumes do not develop since at that location the convective regime is less vigorous. On the other hand, temperature disturbances play a dominant role on brine migration especially in the neighborhood of salt diapirs. A zoom of the calculated pore velocity and temperature fields in a salt dome environment is shown in figure 1.12.

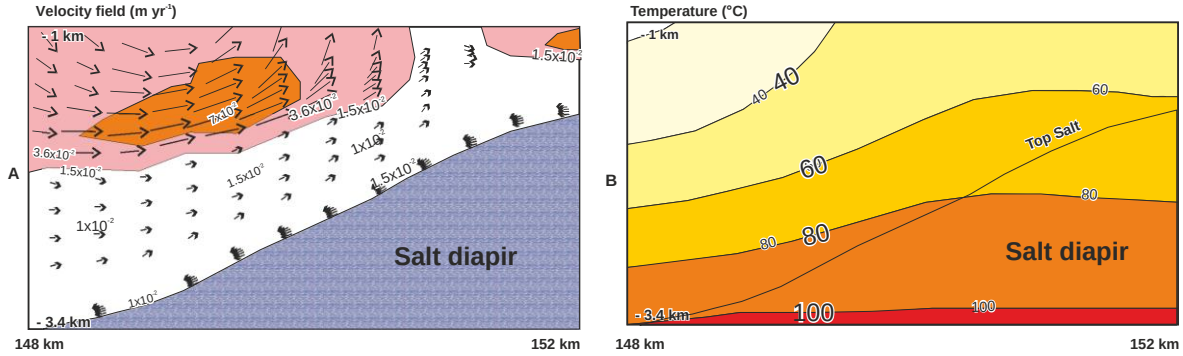

Fig. 1.12: Zoom of thermohaline simulation results in the salt dome environment. A: Pore water velocity field in m yr^{-1}. Pore vector linearly scaled to the flow arrow. B: temperature distribution in °C

Downward forces resulting from the gravitational field control groundwater flow along salt diapir flanks. Brine sinks at approximately 1.5 cm yr-1 (Fig. 1.12A). By contrast, an upward flow paralleling this descending flow occurs in the overlying unit at approximately 1 cm yr-1. This phenomenon can be explained by the temperature distribution (Fig. 1.12B). Because of the thermal conductivity contrast between salt and overlying sediments the isotherms are convex near the edge of the salt diapir. The increased temperature gradient causes a decrease in fluid density near the salt dome. This drives the groundwater flow toward the salt dome and initiates the uprising circulation of brine within the neighboring sediments.

So far, the thermohaline regimes have been illustrated in deep salt diapirs environment. However, salt structures are often shallow. By instance diapir crests close to the basin surface provide a source of high salinity for shallow groundwater which becomes denser than the underlying fluids. As a result, completely different scenarios for thermohaline convection than those previously described can occur. Here, a numerical simulation is run along a profile of a shallow salt diapir of the NEGB. This structural profile includes a steep salt diapir piercing the sediments up to the surface. The results are illustrated in figure 1.13.

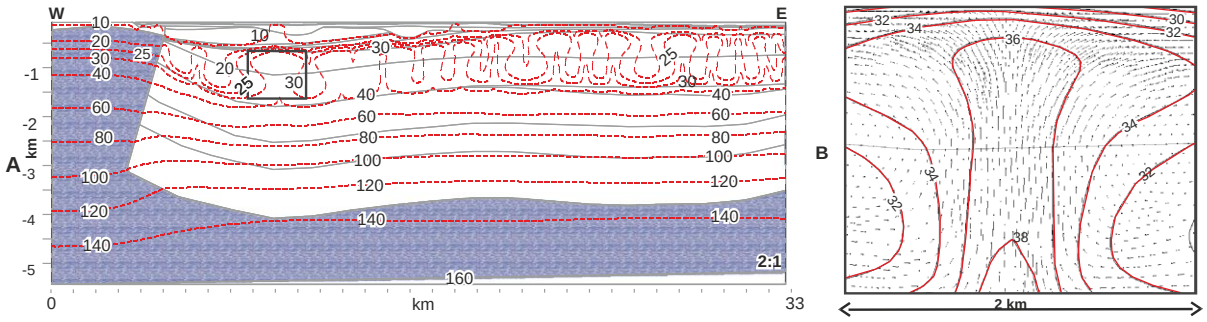

Fig. 1.13: Coupled fluid flow and heat transport simulation in a shallow salt dome. A: Calculated temperature profiles in °C (red lines). Black lines delimit the stratigraphic succession. The upper units are the Palaeogene and the Cretaceous aquifers B: Zoom of the thermally induced plumes without vertical exaggeration. Black vectors indicate the flow direction.

Different regimes developed within the profile. Within the salt unit, the thermal regime is conductive. Again, owing to the strong contrast between the thermal conductivity of the salt and the neighbouring sediments, concave isotherms are found within the salt diapir while convex above the salt. According to the Rayleigh theory in a porous media, the onset of multi-cellular convection is favoured in thick and permeable units (Nield 1968). This is the case for the Palaeogene and the Cretaceous units where a thermally induced convective regime controls the flow. Thermal plumes of 1.5 km height rise vertically from the Cretaceous basis up to the surface, bounded by the regional flow. A zoom of an ascending thermal plume is shown in figure 1.13B. The cell radius is 1 km and the flow rate in the central part of the plume is few millimetres per day. In the deeper units the isotherms are not perturbed and the regime is conductive. Temperature and salinity profiles are shown in figure 1.14

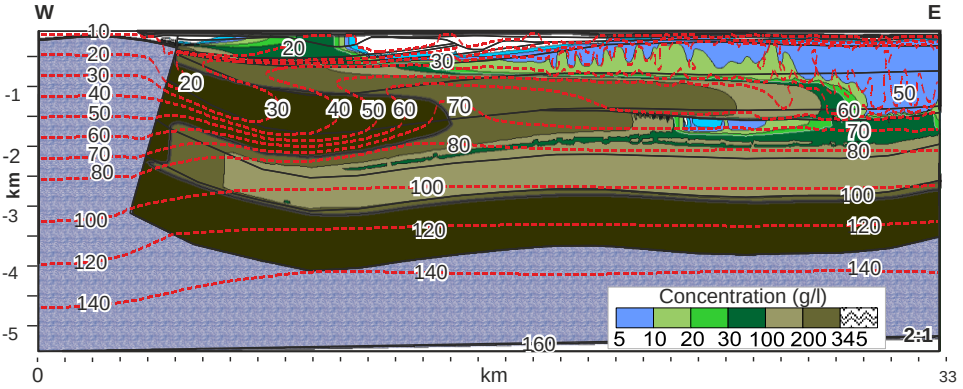

Fig. 1.14.: Thermohaline simulation in a shallow salt dome. Calculated mass (filled patterns, g/L) and temperature profiles (red dashed lines, °C). Black lines delimit the stratigraphic succession. The upper units are the Palaeogene and the Cretaceous aquifers.

Highly saline brines protruding from the salt diapir into the Cretaceous overwhelm the less intense thermal convective regime. Heat plumes do not stretch vertically but develop almost horizontally in the brine flow direction (compare Fig. 1.13 and 1.14). Therefore, the temperature gradient increases horizontally from the salt flank toward the center of the profile. As a result, the temperature field can undergo several inversions with increasing depth in the western part of the profile. In the Eastern part of the basin, thermohaline convection persists within the upper units. Above the horizontally stretched plume, the temperature oscillations generate small convective brine cells (half kilometre radius). As a result, thermally driven saline waters ascend up to the shallow aquifer and spread locally at several points of the surface. In summary, the numerical models have shown that thermally-induced flow is an important process in salt bearing basins, and strongly controls both temperature and concentration gradients. Owing to the presence of thick salt structures, the geothermal field is disturbed. The salt-induced thermal disturbances in turn induce convection of deep brines. However, it is not the only process. Topography-driven flow also influences the geothermal field and can significantly contribute to brine migration. Whereas the principal effects of thermohaline convection could be shown, much more detailed knowledge of transport properties (hydraulic permeability, thermal conductivity) and their regional distribution, including faults and fractures, are necessary in order to achieve more accurate large-scale models.

In the next example, we will how the presence of highly permeable faults can generate convective like groundwater motions also in the surrounding units, possibly being a mechanism causing seawater intrusion in the coastal aquifers of geothermal systems.

The Seferihisar-Balcova Georthermal area (SBG) example

Here, transport processes are numerically investigated in the faults of the Seferihisar-Balçova Geothermal system (SBG), Western Anatolia. In this hydrothermal system, natural springs at temperatures ranging between 30 and 78 °C form along the major faults. An interesting feature of this system is the regional variable salinity of springs: in in the Balçova area, thermal waters have low chloride (Cl) contents, whereas in the, in the Doğanbey area, thermal waters are salty with a strong seawater contribution.

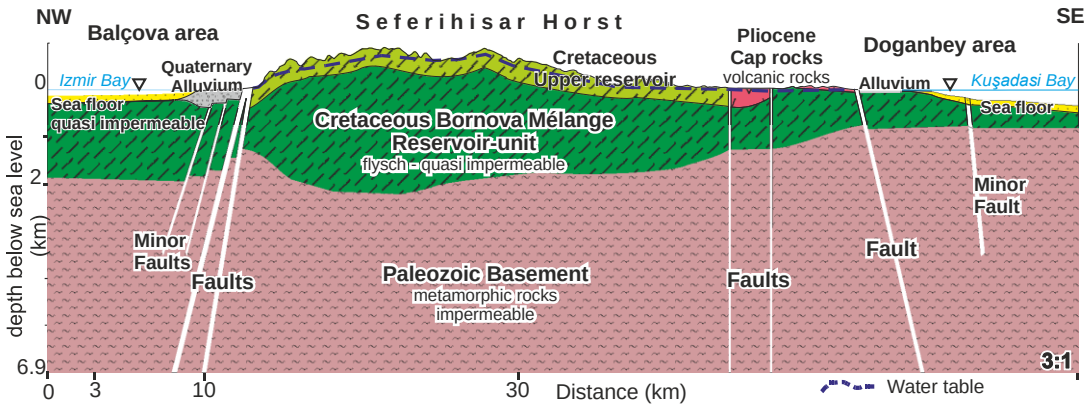

Fig. 1.15.: The Seferihisar-Balçova geothermal system. Geologic setting of the studied profile.

Furthermore, it is not clear what forces drive salty water inland. A DFG project (MA4450-1) was funded to build up the first models of coupled fluid processes in the SBG. The

simulation results indicate that large-scale free convection induced by buoyancy-driven flow develops in all faults driving hot basinal fluids from the basement to the surface.

Simulated flow paths and velocity fields in the Balçova and Doğanbey areas are illustrated in Figure 1.16. Three flow patterns can be distinguished: (1) In the Balçova area, the steep topography gradients drive groundwater from the horst to the coastal alluvium (i.e. regional flow, blue lines). The main discharge zone is the seafloor / alluvium interface. The steep topography gradients lead to very vigorous flow in the alluvium, with peak velocities of 15 m year-1 (Fig. 1.16a).

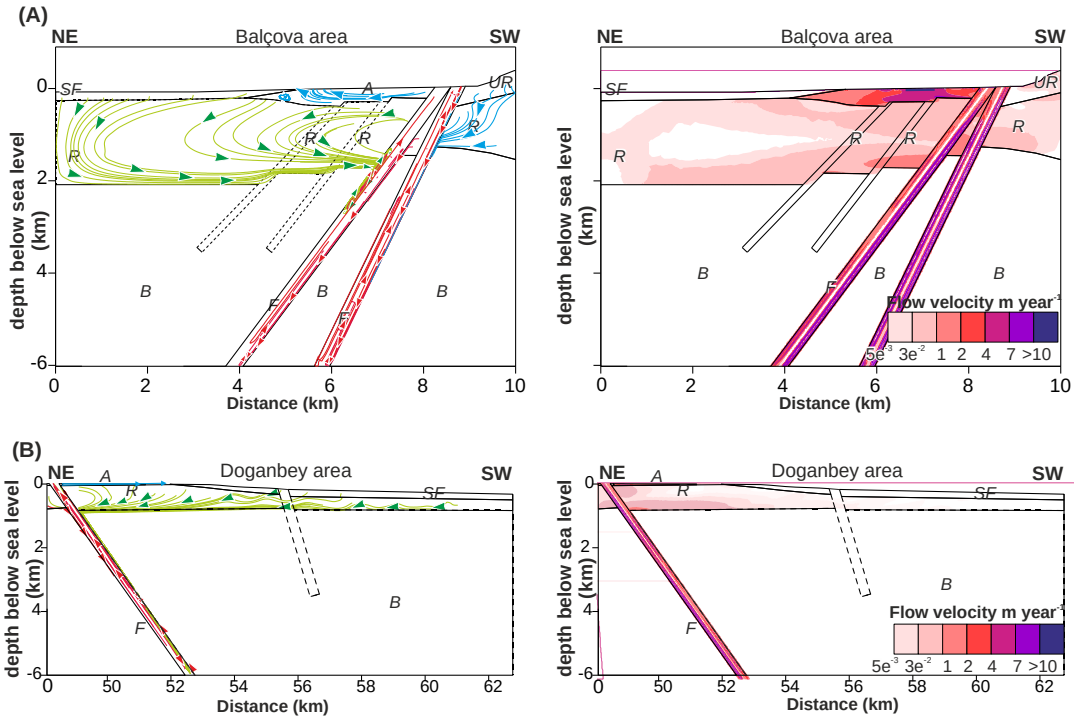

Fig. 1.16.: Flow pathlines (no streamlines) and velocity field (m/year) calculated from transient thermohaline simulations for: (a) Balçova, Northern SBG; and (b) Doğanbey, Southern SBG. The arrows indicate the flow direction. Red flow patterns are free-thermally induced cells in the faults. The resulting fault-induced cells are illustrated in green. Recharge flow from the horst is in blue. Minor faults (dashed lines) are not included in the simulations. (SF: sea floor; A: alluvium; UR: Upper Reservoir; R: reservoir unit, Bornova Mélange; B: basement; F: fault; NE: northeast; SW: southwest). No vertical exaggeration is used

Recharge water also infiltrates through the upper reservoir units into the adjacent fault at velocities of a few centimeters per year. In Doğanbey, the regional flow is extremely weak because of the rather flat topography and the presence of very thin alluvium. (2) In the faults, convective cells (red lines) develop as a result of thermal-buoyant forces; groundwater percolates from the horst to great depths where it is heated by the geothermal gradient. The warm and less-dense water ascends along the faults and vents through alluvium. The velocities of these fault-bounded convective cells range between 2 and 7 m year^{-1} (Fig. 1.16). As a result of the focused outflow of thermal water, the fluid pressure in the faults from the basement to the lower reservoir interface is less, compared to what it would be if cooler waters were in the fault. These pressure offsets are also referred to as pressure drops. (3) As a consequence, in the reservoir unit kilometer-scale flow patterns similar to convective cells (green lines) stretch from the seafloor and alluvium units toward the fault.

Groundwater motion in the reservoir units is driven by the pressure-gradient forces resulting from the constant head at the seafloor and the thermally-induced pressure drop in the faults. In other words, the free convective regime in the faults induces convective-like recirculation in the surrounding units. Simulations without faults do not show convective

circulation, but only topography-driven flow originating from the horst. Because of the impervious nature of the basement, the flow lines run parallel to the upper-basement boundary before they are captured by the convective flow in the fault. As a consequence, fault-induced convection cells are well- developed in the 2-km thick Balçova reservoir, but are poorly defined in the thin aquifer above the uplifted basement in the Doğanbey area. The fault-induced flow velocities range from a centimeter per year near the seafloor to half a meter per year at the edge of the fault (Fig. 1.16).

The described flow patterns have major impacts on both the temperature (Fig. 1.17) and mass distribution (Fig. 1.18) in the profile. The ascending buoyant plumes generate elevated temperature within the faults (Fig. 1.17). As a result, the isotherms within the faults are deflected parallel to the fault leading to several temperature inversions. Temperatures higher than 80 °C occur locally within the alluvium at fault intersections where thermal waters vent. In the Balçova area, the vigorous regional flow generates a thermal plume that reaches 50 °C upon discharging at the ground surface. Advected thermal plumes of this nature are unlikely to develop in the Doğanbey area, where the regional flow is less vigorous. Far from the faults, the geothermal gradient is purely conductive, suggesting that the fault-induced cells are not generated by the geothermal gradient of the basin (i.e. there is no free convection). The onset of thermohaline convection can be determined by calculating thermal and solutal Rayleigh numbers. However, an accurate stability analysis of transient large-scale models is challenging, if not impossible, because the physical properties of fluid and hydrogeologic units are not constant. Several simulations in which the reservoir permeability has been gradually increased showed that the onset of thermal convection is triggered in the Balçova and Doğanbey reservoir units at hydraulic conductivities of 17 m year^{-1} and 32 m year^{-1} respectively.

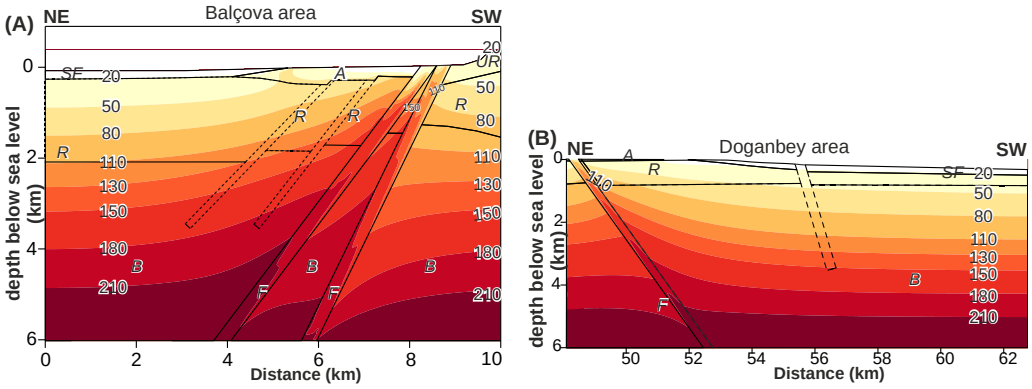

Fig. 1.17: Temperature (°C) calculated from transient thermohaline simulations for: (A) Balçova, Northern SBG; and (B) Doğanbey, Southern SBG. Minor faults (dashed lines) are not included in the simulations. (SF: sea floor; A: alluvium; UR: Upper Reservoir; R: reservoir unit, Bornova Mélange; B: basement; F: fault; NE: northeast; SW: southwest)

The vigorous upward flow in the faults can induce km-scale convective cells in the surrounding Mélange, as explained previously (Fig. 1.17). These fault-induced convection cells develop in areas where the regional flow is weak, such as below horizontal alluvium deposits and seafloors.

In the latter case, the convection cells that extend to the freshwater/seawater interface can drive salty waters toward the faults and inland units (Fig. 1.18).

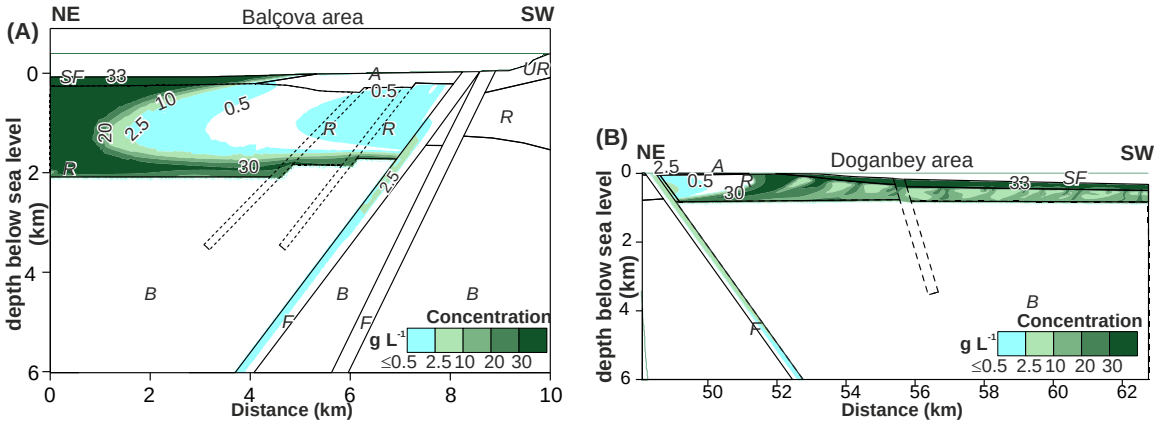

Fig. 1.18: Concentration (gL^{-1}) calculated from transient thermohaline simulations for: (A) Balçova, Northern SBG; and (B) Doğanbey, Southern SBG. Minor faults (dashed lines) are not included in the simulations. (SF: sea floor; A: alluvium; UR: Upper Reservoir; R: reservoir unit, Bornova Mélange; B: basement; F: fault; NE: northeast; SW: southwest)

The results show that at the fault intersections, seawater mixes with ascending thermal waters. The salinity of the resulting springs is likely controlled by different flow rates of the regional flow and structural features of the basin: In the northern area, extended areas of low TDS are due to both the strong topographic gradients and thick deposits of alluvial and Mélange sediments. By contrast, in the south, the flat topography, thin alluvium, and the uplifted basement reduce the depth of seawater penetration and favour the merging of plumes into wide saline areas. In the Balçova area, a 30 g L-1 seawater finger stretches from the seafloor toward the fault (Fig 1.18a). In the Doğanbey area, several heavy plumes sink within the longer and thinner reservoir unit (Fig. 1.18b).

A coupled fluid-flow and mass-transport simulation showed that without a geothermal gradient the initial linear salinity distribution within both seafloors remains unchanged. Therefore, the seawater plumes in the reservoir units do not result from density-driven convection, in which a denser fluid sinks into an underlying lighter fluid, but from the forced convection induced by the hydraulic head patterns.

Though this part illustrates the SBG example, the described processes concern faults which can be encountered in many geothermal systems in the world. The described fault-induced convection cells could by example explain outflow of relict brine through the faults of the Tiberias Lake, the presence of dissolved halite within the faults of the Rhine Graben, Germany or the mineral deposits in the Polish Basin.

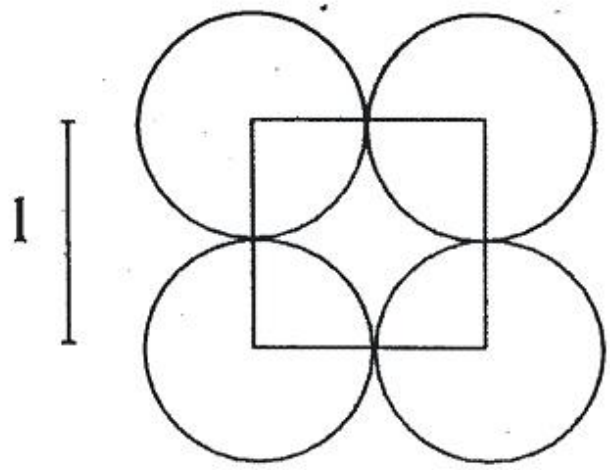

$$V_{zelle} = l^3$$

$$T_k = 1/2$$

$$V_k = \frac{3}{4}\pi\left(\frac{l}{2}\right)^3 \approx 4.189\left(\frac{l}{2}\right)^3 = 0.523$$

$$\phi = \frac{l^3 - V_k}{V_{zelle}} = 1 - \frac{V_k}{V_{zelle}} = 0.477$$

Min 0.259 % dichteste Packung

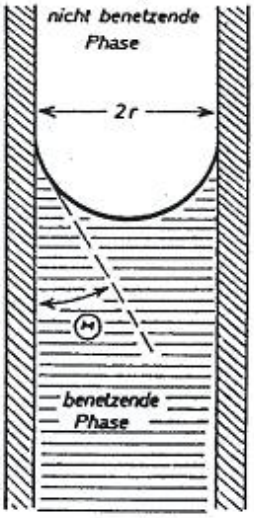

Abb. 5-7. Zur Definition des Kapillardrucks (Erklärung im Text).

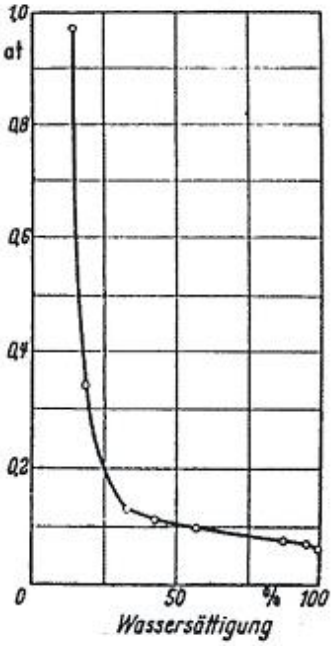

Abb. 5-8. Kapillardruckkurve eines feinkörnigen Sandsteins.

$$P_c = \frac{2\gamma \cos\Theta}{r}$$

in der schlechter benetzenden Phase herrscht der höhere Druck

γ: Grenzflächenspannung

z. B. Wasser/Öl = 25 dyn/cm

Wasser/Gas = 70 dyn/cm

Wasser (benetzend) hat den Randwinkel

$$\Theta = 0$$

Daraus errechnet sich die Tabelle.

Sediment	r	PCO	PCG
	[cm]	[at]	[at]
Ton	10^{-5}	5	14
Silt	10^{-4}	0,5	1,4
Sand	10^{-3}	0,05	0,14

Permeabilität

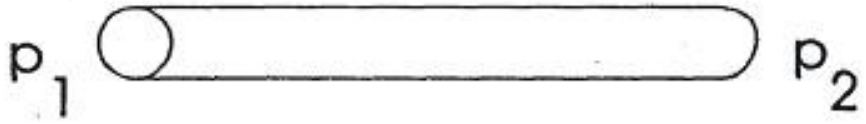

Fluß durch eine Kapillare
HAGEN - POISEUILLE:

$$q = \frac{i^2}{8\mu} \cdot \frac{\Delta p}{l}$$

Verallgemeinerung

$$q = \frac{m^2}{c_o} \cdot \frac{1}{\mu} \cdot \frac{\Delta p}{l}$$

$$m = \frac{\text{Volumen}}{\text{Oberfläche}}$$ der Kapillare

c_o ein Formfaktor

für Kreis = 2
für Rechteck = 2,65

Effektiver Querschnitt

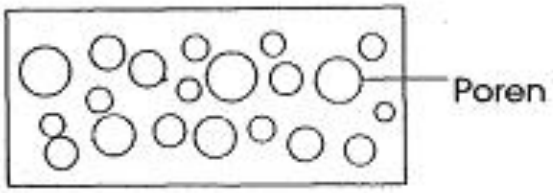

Tortuosität:

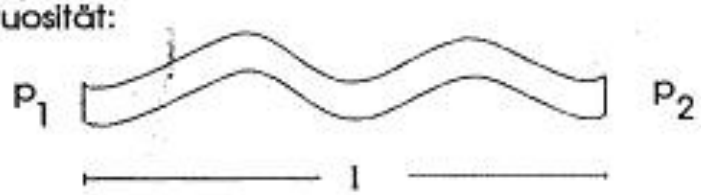

$$\Rightarrow q = \frac{m^2 \phi}{c_o}\left(\frac{l}{l_e}\right)^2 \cdot \frac{1}{\mu} \cdot \frac{\Delta p}{l}$$

Abschätzung:

$$m = \frac{\phi}{(1-\phi)s_o}$$

ϕ: Volumen der Kapillaren
S_O: Oberfläche der Kapillaren

$\Rightarrow$ KOZENY-CARMAN Gleichung

$$q = \frac{\phi^3}{(1-\phi)^2} \cdot \frac{l^2}{s_o^2 c_o l_e^2} \cdot \frac{1}{\mu} \cdot \frac{\Delta p}{l}$$

$$c_o l_e^2 / l^2 \approx 5$$

Kugelpackungen: $$k = \frac{\phi^2}{5(1-\phi)^2 s_o^2}$$